RSC Advances

ROYAL SOCIETY OF CHEMISTRY

www.rsc.org/advances

Structure-Property Relationships in Super-Toughened Polypropylene-Based Ternary Blends of Core-Shell Morphology

Majid Mehrabi Mazidi[1,2], Mir Karim Razavi Aghjeh[1,2]*, Hossein Ali Khonakdar[3], Uta Reuter[3]
[1]Institute of Polymeric Materials, Sahand University of Technology, Sahand New Town, Tabriz, Iran P.C: 51335-1996
[2]Faculty of Polymer Engineering, Sahand University of Technology, Sahand New Town, Tabriz, Iran P.C: 51335-1996
[3]Leibniz Institute of Polymer Research Dresden, D-01067, Dresden, Germany
*Correspondence to: Dr. M.K. Razavi Aghjeh
Email: karimrazavi@sut.ac.ir

Abstract

Structure-property relationships in PP/EPDM-g-MA/PA6 (70/15/15) ternary blends were studied in detail. PP-based reactive ternary blends with greatly improved impact strength were obtained via manipulation of phase morphology by applying different processing methods. SEM and TEM techniques were employed to study the phase morphology, which was shown that played a significant effect on the different properties, especially the tremendous improvement of the impact toughness. Reactive ternary blends showed core-shell morphology (core: PA6, shell: EPDM-g-MA in PP matrix) with quite different dispersed structures, in the form of mainly individual core-shells, clusters of core-shell particles, or percolation of clusters. Phase compatibility and thermal properties of the blends were studied by DMA and DSC analysis. A super-toughened PP-based reactive ternary blend with the impact strength much higher than PP/EPDM (70/30) binary blend and about 15 times higher than that of pure PP was achieved. This was ascribed to a unique "percolated" structure of core-shell particles in the matrix, indicating the importance of dispersion state of modifier particles in enhancing the impact strength. Fracture behavior and toughening micro-mechanisms were rationalized by post-mortem fractography of the impact-fractured surfaces. Synergistic effects of interconnected structure and suitable interfacial adhesion together with cavitation and irreversible plastic growth of micro-voids caused massive shear yielding of the matrix material in the super-toughened blends.

Keywords: Core-Shell Morphology; Percolated Structure; Properties; Impact Toughness; Shear Yielding

1. Introduction

The melt blending of two or more polymers provides an easy and efficient way to generate new polymeric materials with novel and targeted properties at a relatively low cost compared to developing a new polymer.[1-10] It is well-known that the different properties of polymer blends greatly depend on the phase morphology. Hence, the control and the prediction of morphologies for the optimization of desired properties has always been a research focus.[8-15] In multiphase polymer systems the phase morphology is generally determined by the following factors: material characteristics (interfacial tension between different components and rheological properties of the blend constituents) and processing conditions (mixing time and temperature, the type and the extent of deformation flow field and the feeding order of different components).[8-15] In other words, the morphology of polymer blends is controlled by the thermodynamic and kinetic factors.

The great majority of useful polymer blends are immiscible, and their outstanding performance stems from their multiphase morphologies. Stabilization of the blend morphology, or compatibilization as it is usually termed, involves modification of the interfacial properties of the blend. The compatibilizing agents are usually either formed in situ, by reactive compatibilization, or are pre-formed and incorporated in a separate step.[16-19] Reactive compatibilization provides a degree of control over morphology development in multiphase polymer blends, via manipulation of the interfacial energies within the system, which allows the formation of a composite dispersed phase during a melt blending process via encapsulation of one dispersed phase by another.[16-19] In most cases, the formation of core-shell structure is related to interfacial tensions between different polymer pairs or the minimization of surface free energy of polymer blends.

In the case of ternary polymer blends containing three mutually immiscible polymeric components, the majority of the works in the literature have focused on the control and prediction of the phase morphology developed during the melt blending.[8, 11-14, 20,21] A literature survey shows that there is an increasing tendency in recent years towards understanding how the different phase morphologies, developed in multiphase systems, affect the various morphology-dependent properties of the final material.[22-34] Blends of polyolefins with polyamides, when properly compatibilized can combine some of the best characteristics of both materials: good chemical resistance, low water sorption, high heat deformation temperature and reduced cost.

Since the toughness is an important selection criterion for many engineering applications, improvement of toughness in polyolefin/polyamide blends with little loss in other desirable mechanical properties is also of great importance. Li et al.[24,25] investigated the role of core-shell structure on the different properties of PA6/EPDM-g-MA/HDPE ternary blends. They used two processing methods to prepare the reactive ternary blends and then the dependence of the phase morphology on interfacial interaction and processing method was discussed. The core-shell morphology with thicker EPDM-g-MA shell, developed in the blend prepared by two-step method, resulted in a super toughened PA6 ternary blend. Yin et al.[28] further studied the effect of shell thickness on the fracture toughness of PA6/EPDM-g-MA/HDPE ternary blends. The results suggested that the fibrillation of core-shell particles, as "Particles Bridge", can absorb fracture impact energy and sustain a higher stress to obtain the effect of strain hardening and prevent further propagation of micro-crack, and thus obtain higher notched Izod impact strength.

There are numerous research works on the structure and properties of PP-base PP/PA6/elastomer ternary blends in the literature.[17-19,35-49] Most of these works have utilized SEBS-g-MA, polyolefin elastomers (such as poly(ethylene-co-octene)) and PP-g-MA as compatibilizer and/or toughening agent. In our previous work,[49] we investigated the effect of blend composition and compatibilization (by using PP-g-MA) on the morphology, mechanical properties and quasi-static fracture toughness of PP/PA6 blends toughened with nonfunctionalized EPDM. Little works have been reported on PP-matrix PP/PA6 blend systems containing functionalized EPDM-g-MA as toughener.[50,51] Shokoohi et al. [50,51] studied the phase morphology and mechanical properties of PP/(EPDM+EPDM-g-MA)/PA6 70/(7.5+7.5)/15 blends prepared using a twin screw extruder. They reported optimum processing conditions in terms of tensile and impact properties. However, they did not report the amount of improvement in impact toughness of the prepared blends under the optimum conditions as compared with that of pure PP matrix. Further studies on the structure-property relationships in these systems are beneficial to obtain a deeper understanding of the different morphologies develop in these blends and their impact on the materials' performance. Moreover, more detailed analysis of the failure behavior and micro-mechanical deformations operating in these systems could also provide a basis for designing highly-toughened materials with engineering applications.

To get more insight into the PP-matrix PP/PA6 blends toughened by EPDM-g-MA, the present work was aimed to investigate in detail the microstructure and properties of PP/EPDM-g-

MA/PA6 (70/15/15) ternary blends using various analyses. The influence of mixing order on the phase morphology development and its effects on different properties, especially the impact toughness, was thoroughly investigated. Attempt was made to establish structure-property correlations in the blends studied. Super-toughened reactive blends were obtained with quite different phase morphology and dispersion states of modifier particle compared with the systems reported earlier. Fracture behaviors were studied in detail along with fractography analysis of impact-fractured surfaces and as a result the toughening micro-mechanisms were proposed.

2. Experimental

2.1 Materials

PA6 used in this study was Tecomid NB40 NL E. The isotactic polypropylene (iPP: SF 060, MFI=5.0 g/10 min; 230°C and 2.16 Kg) was obtained from Polynar Petrochemical Co., Tabriz, Iran. Ethylene-propylene-diene rubber grafted with maleic anhydride (EPDM-g-MA, denoted as mEPDM in the text), with the trademark of TRD-359EP, was purchased from Yangzhou Henghui Chemical Co., LTD, with Moony viscosity (ML 1+4, 100°C) of 23, mass density of 0.875 g/cm^3 and MAH content of about 1.1 wt%.

2.2 Sample preparation

PA6 and EPDM-g-MA were vacuum-dried for 12 h at 80 °C before blending to eliminate the effects of moisture. Different processing procedures were employed to prepare the reactive PP/EPDM-g-MA/PA6 (70/15/15) ternary blends. One was called *one-step processing method (denoted as TR1 in the text)*, in which the EPDM-g-MA and PA6 were directly melt blended with PP matrix at starting temperature of 230 °C. In the second method of reactive mixing, the EPDM-g-MA and PA6 were firstly melt blended at a temperature of 230 °C, and then the resulted blend master-batch was blended with pure PP, which was denoted as *TR21*. In the third method of reactive mixing, the EPDM-g-MA and PP were firstly melt blended, and then the resulted blend master-batch was blended with pure PA6 at a starting temperature of 230 °C, and was denoted as *TR22*. Moreover, PP/EPDM-g-MA and PP/PA6 reference binary blends containing of 30 wt% minor components were also melt-blended. A small amount of the prepared blend samples was rapidly quenched in liquid nitrogen for morphological studies. Then

all the blends were compression molded at 230 °C to obtain standard specimens for the tests of mechanical properties.

2.3 Morphological observations

The phase morphology of the samples was studied by field emission gun scanning electron microscopy (FESEM) and transmission electron microscopy (TEM) instruments. For FESEM experiments, the cryo-fractured surfaces, in liquid nitrogen, were gold sputtered for good conductivity of the electron beam and microphotographs were taken within different magnifications. For better understanding of dispersion state of the dispersed phases, a selective extraction was applied to the elastomeric phase domains. For this purpose, the EPDM-g-MA phase was selectively extracted in cyclohexane solvent at room temperature for 24 h. Then, the samples were dried at 85 ˚C in a vacuum oven overnight. For the purpose of particle size analysis, at least 400 particles from independent SEM micrographs were analyzed by using the image processing software (ImageJ, NIH, U.S.A.). The cross-sectional area (A_i) of each individual particle (i) was measured and converted into an equivalent diameter of a sphere using Eq.1 as follows:

$$d_i = 2\sqrt{A_i/\pi} \quad (1)$$

The number-average particle diameter, d_n, and mass-average particle diameter, d_m, were determined using Eqs. 2 and 3 as follows:

$$d_n = \frac{\sum n_i d_i}{\sum n_i} \quad (2)$$

$$d_m = \frac{\sum n_i d_i^2}{\sum n_i d_i} \quad (3)$$

where n_i is the number of particles having the diameter d_i. The particle size polydispersity was represented as the ratio of mass-average particle diameter, d_m to the number-average particle diameter, d_n, that is, d_m/ d_n.

TEM was performed on a Philips EM208 microscope (Netherlands), operated at 100 kV. The samples were microtomed at -160 °C. Specimens of about 80 nm thick were prepared for TEM using a Reichert Ultracut ultramicrotome fitted with a diamond knife, then stained by exposure for 30 min to ruthenium tetroxide vapors generated from the oxidation of ruthenium dioxide by excess sodium periodate at ambient temperature.

2.4 Contact angle measurements

Contact angles were measured in a sessile drop mold with KRÜSS DSA100 (German). PP, EPDM-g-MA and PA6 samples were compression-molded between clean silicon wafers at 240 °C for 5 min and then cooled to 30 °C. Contact angles were measured on 3 ml of wetting solvent at 25 °C, and the mean values of seven replicates were reported.

2.5 Differential scanning calorimetry (DSC)

Thermal behavior of the samples was studied with a Netzsch-DSC 20 0F3 (Germany) instrument under nitrogen atmosphere. Each sample of 10 ± 0.2 mg was taken from a molded sheet and encapsulated in an aluminum closed pan. Samples were first heated from 40 °C to 250 °C at a heating rate of 20 °C/min, held at 250 °C for 5 min to erase any previous thermal history and then cooled to 40 °C at the cooling rate of 10 °C/min and heated again to 250 °C with the 10 °C/min heating rate. The results of cooling and the second heating run (or step) have presented in this work. The % of matrix (PP) crystalline phase (X) was estimated using the following equation:

$$X_C = \frac{\Delta H_m}{w_f \, \Delta H_m^\circ} \times 100 \qquad (4)$$

where ΔH_m is the enthalpy of melting for analyzed sample, w_f is the mass fraction of PP in the blend and ΔH_m° is the enthalpy of fusion for 100% crystalline PP, taking the value of 209 J/g from the literature.[17,18]

2.6 Tensile properties and Izod impact toughness

Tensile tests were conducted on a Zwick/Roell tensile testing machine (Z 010) at a fixed crosshead speed of 5 mm/min at room temperature according to ISO 527. At least four specimens were tested for each composition and the resulting tensile properties were averaged.

The impact toughness of the samples was determined by the notched Izod impact test (Zwick/Roell B5102 pendulum impact tester) according to ASTM D256. The results of the impact strength are the average of at least six repetition obtained at a temperature of 25 °C.

2.7 Dynamic mechanical analysis (DMA)

DMA was conducted on a DMA Q800 from TA Instruments using a dual-cantilever clamp with a mode of frequency sweep/temperature ramp at the frequency of 1 Hz and oscillating amplitude of 15 μm. The samples (dimensions 12.7 × 63.5 × 3.2 mm) were heated from −140 to 150 °C at a heating rate of 3 °C/min.

2.8 Fractographic analysis

To elucidate the role of phase morphology on the fracture behavior of the samples, and also to understand the micro-mechanisms of deformation related to the different systems, FESEM micrographs were also taken from the surface of impact-fractured specimens of different samples.

3. Results and discussion

3.1 Phase morphology of the blends

It is well-known that the properties of multiphase polymer blends are strongly dependent on the phase morphology. Therefore, study of the microstructure and dispersion state of minor components in the blends prepared in this work, is of prime importance, which subsequently is useful for an attempt to establish the relationship between the morphology and the resulting performance. The SEM micrographs of PP-based binary blends are presented in **Figure 1**. The particle size distribution curves of the binary blends are also shown in that figure. For PP/PA6 and PP/mEPDM binary blends, the typical matrix-disperse type morphology is clearly visible, which is characteristic of immiscible binary systems. Owing to incompatibility of the components in PP/PA6 blend, the dispersed PA6 domains are unstable toward coalescence during processing, leading to large PA6 particles size (number-average diameter of about 7 μm). There is also evidence of poor interfacial bonding in PP/PA6 system with PA6 particles detached

from the surrounding matrix leaving holes and/or lying loose on the surface after the fast cryogenic fracture. It is also obvious that the mEPDM rubbery phase shows much finer dispersion in the PP matrix (number-average diameter of about 2 μm). This is due to relative compatibility of mEPDM component with the PP phase.

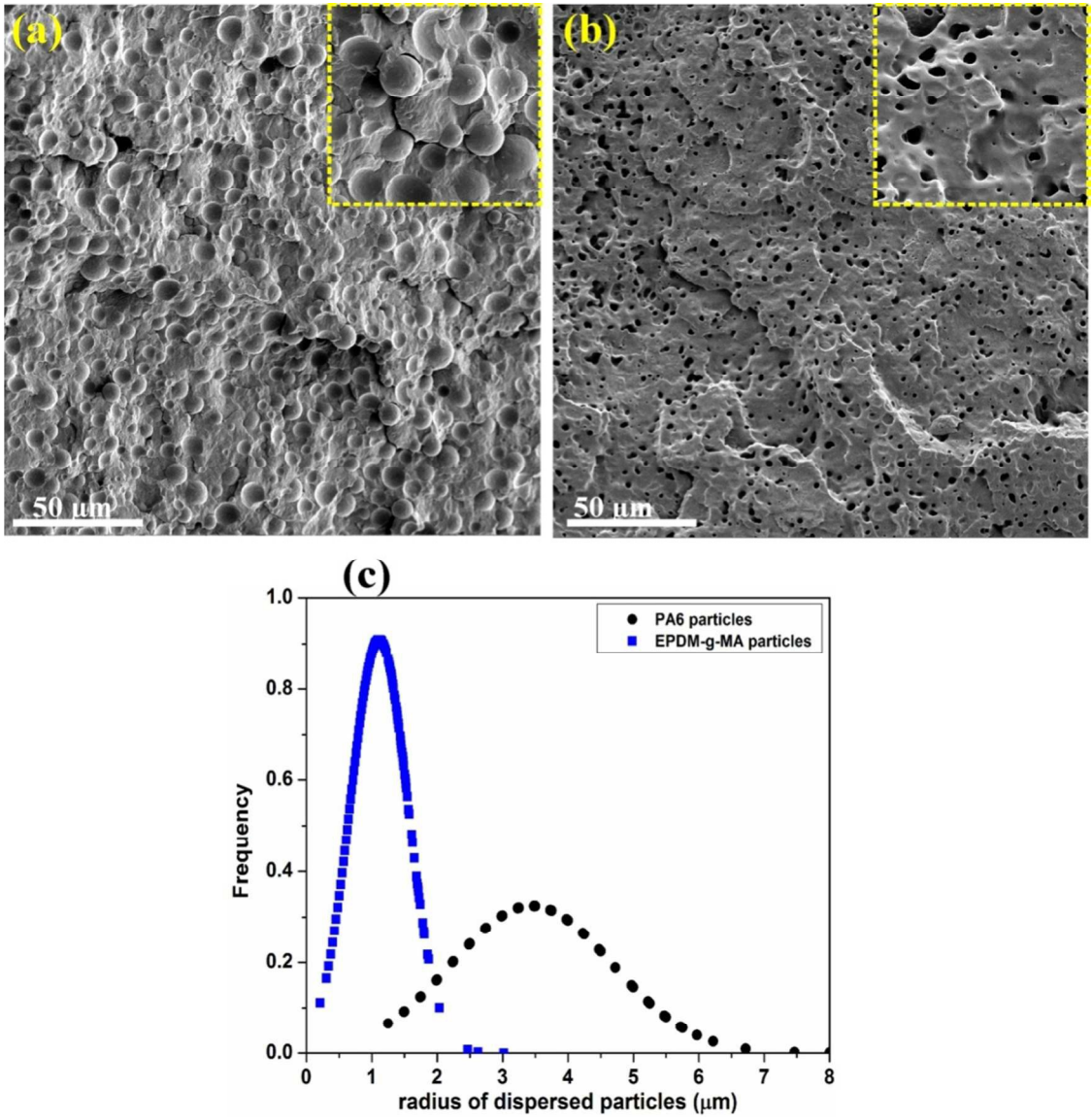

Fig. 1: SEM micrographs of cryofractured surfaces of different binary blends. (**a**) PP/PA6 (70/30); (**b**) PP/mEPDM (70/30) with mEPDM etched by cyclohexane. (**c**) particle size distributions for dispersed component.

The SEM images of cryogenically-fractured surfaces of PP-based reactive ternary blends are depicted in **Figure 2**. The reactive ternary blends exhibit dispersed structures composed of relatively small PA6 phase domains having obscure interfacial region with the surrounding

matrix material. This is due to the fact that in these ternary blends, the mEPDM distributes mainly at the interfacial region between PA6 dispersed domains and PP matrix, and PA6 particles become encapsulated by mEPDM phase.

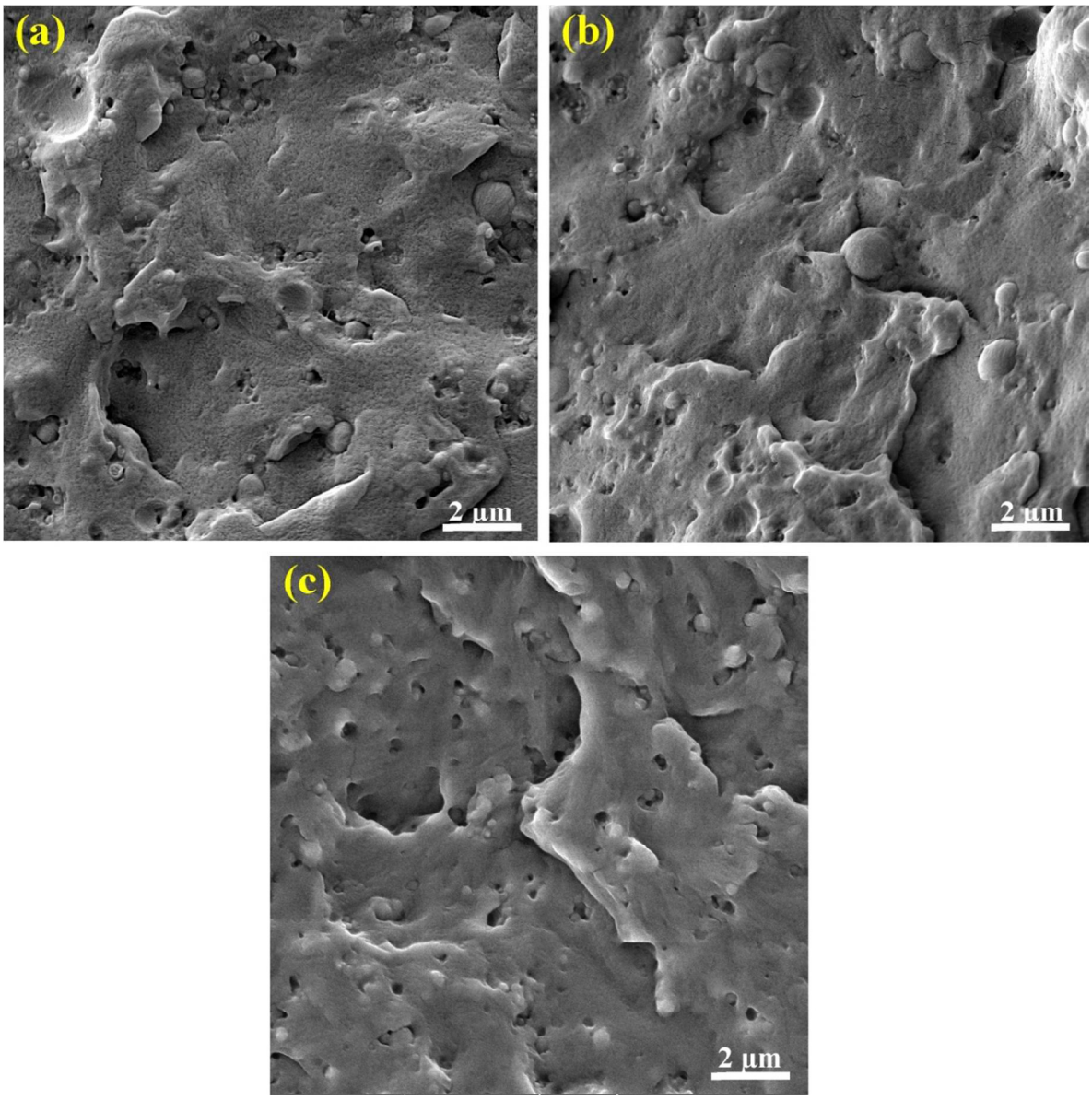

Fig. 2: SEM micrographs of cryofractured surfaces of PP/mEPDM/PA6 (70/15/15) reactive ternary blends. (**a**) TR1 blend; (**b**) TR21 blend; (**c**) TR22 blend.

It is well documented that during the melt mixing process, the maleic anhydride groups of mEPDM react with amine end groups (or amide linkages) of PA6 chains, leading to the *in-situ* formation of EPDM-g-PA6 copolymer at the interfacial region between PA6 and mEPDM. As an effective interfacial layer, the formed graft copolymer significantly reduces the interfacial

tension between the PA6 and PP matrix, with subsequent increase in the interfacial adhesion. Close examination of the micrographs in **Figures 2a-c** further revealed that in these ternary blends, the phase morphology is highly affected by the mixing procedure. It is clearly visible that the size of PA6 particles, their dispersion state in the matrix, and the degree of interfacial adhesion between the components and the matrix are greatly influenced by the mixing order.

Figure 3 shows the SEM images taken from the cryo-fractured surfaces of ternary blends in which the rubbery phase has been etched prior to microscopic imaging.

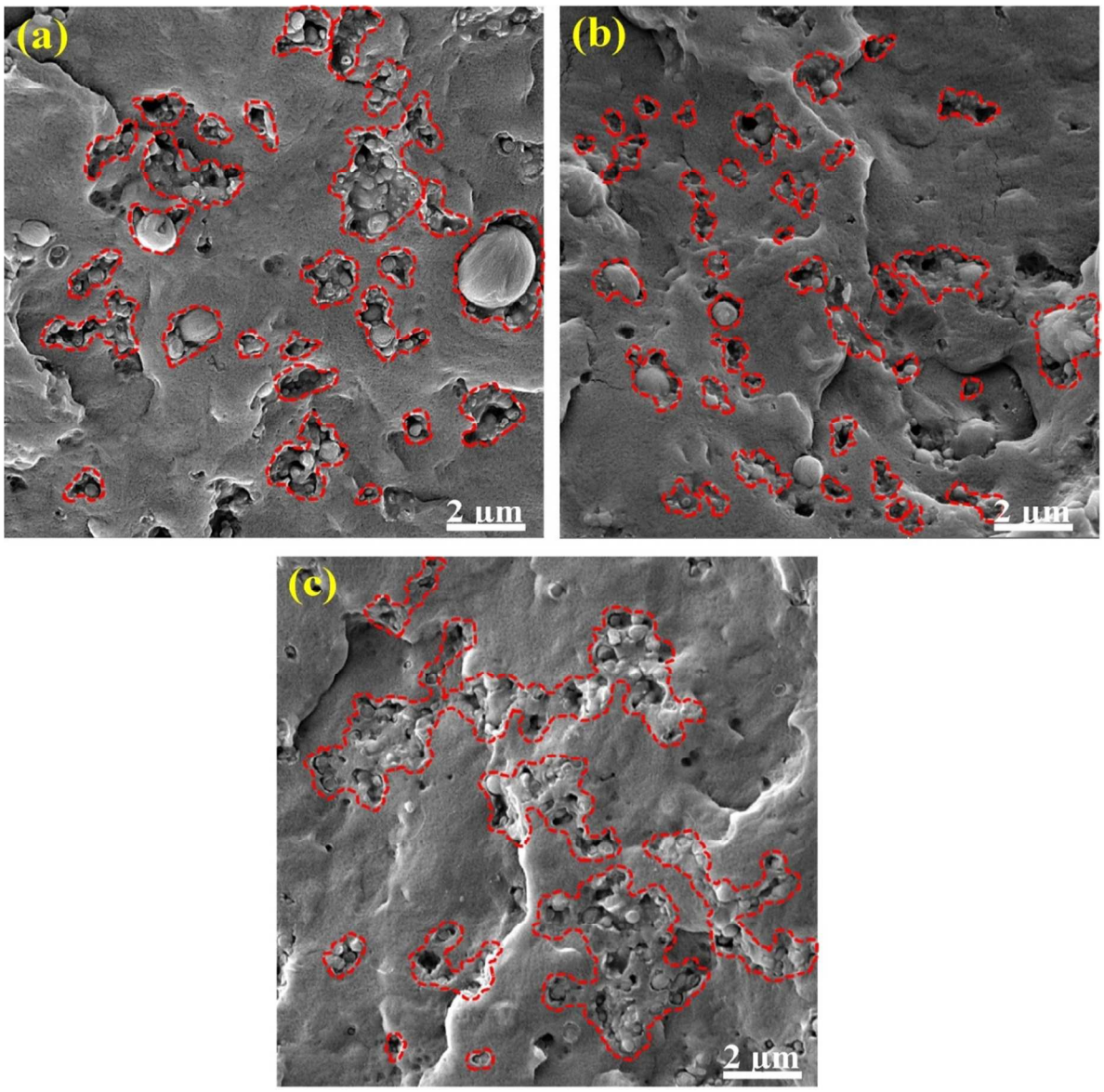

Fig. 3: SEM micrographs of cryofractured surfaces of PP/mEPDM/PA6 (70/15/15) reactive ternary blends. (**a**) TR1 blend; (**b**) TR21 blend; (**c**) TR22 blend. The mEPDM was etched by cyclohexane.

In the case of TR1 blend system, the micrograph in **Figure 3a** reveals that the dispersed phase domains are composed of PA6 particles which are agglomerated and joined together in the matrix. This is much similar to a "sea-island" type phase morphology. By considering the high reactivity of mEPDM towards PA6 phase in reactive ternary blends and that the micrographs are related to the etched samples, it can be concluded that the island-like phase structures developed in the ternary system in **Figure 3a** are consisted of the agglomerated PA6/mEPDM core-shell particles, which may be further surrounded by a layer of rubbery phase to form clusters in the matrix. A small number of large PA6 particles either in the form of isolated domains or included within the clusters are also visible in the micrograph. It should be noted that no separate micro-phase formation of mEPDM phase in the matrix could be detected in the micrograph of **Figure 3a**.

For TR21 blend, **Figure 3b** shows the presence of relatively large PA6 dispersed droplets together with some phase domains which seems to be consisted of association of PA6 particles with very small particle size. Therefore, the phase morphology of the reactive ternary blend fabricated by two-step mixing (1) is composed of the mainly individual core-shell type dispersed particles, together with small aggregates of these particles. However, the aggregated structures formed in this system are much smaller in size and seems to have lower content of both PA6 and rubber phases as compared with those formed in reactive blend prepared by one-step mixing procedure. Moreover, comparing the micrographs of **Figure 3a** and **Figure 3b** represent that a larger number of isolated big PA6 particles are presented in the TR21 ternary blend than the TR1 blend. These findings indicate a different dispersion state of minor components in the reactive ternary blends prepared by one- and two-step mixing (1) methods.

In contrast with the phase structure of TR1 and TR21 systems presented above, a homogeneous and much more uniform distribution of agglomerated core-shell particles are developed throughout the matrix material in the TR22 sample, i.e. reactive ternary blend prepared by two-step mixing (2) (**Figures 2c, 3c**). This type of dispersion state resembles to an "interconnected" phase structure, which seems to form when the percolation of core-shell clusters takes place in the material. As can be seen, the dispersed PA6 particles within the interconnected structures have much more uniform size distribution than those in the other reactive ternary blends, i.e. TR1 and TR21.

Figure 4 shows the typical phase morphologies of TR1 and TR22 reactive blend systems studied by TEM technique. In these micrographs, it is apparent that the phase structure of modifier particles corresponds to that of core-shell structures of ternary systems, in which the PA6 particles as the core phase surrounded by mEPDM rubbery phase as the shell (stained black by the action of the RuO_4) are dispersed in the PP matrix. As stated earlier, this is due to the reaction between the maleic-anhydride grafts on the elastomer and the terminal amine groups of PA6.

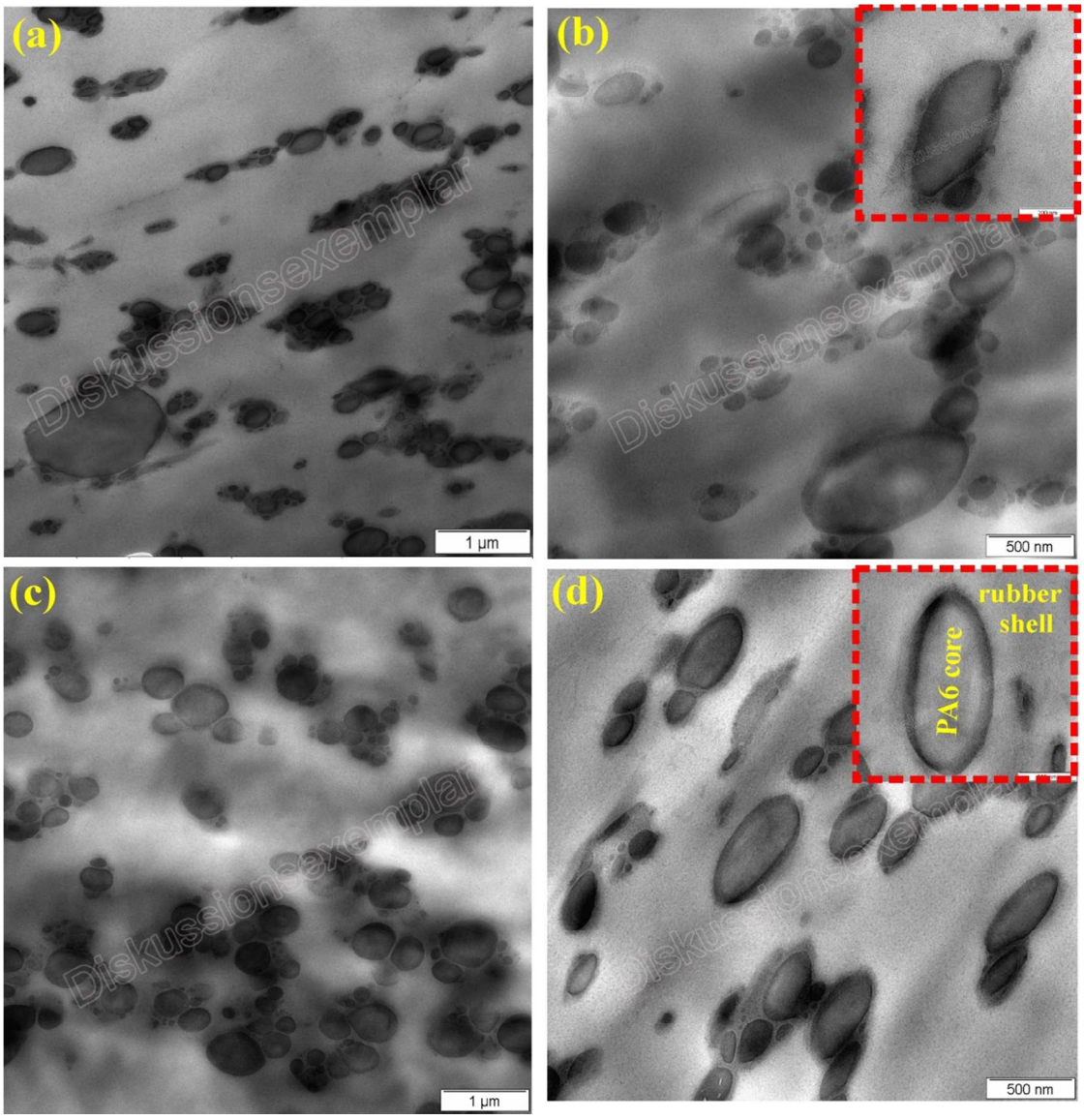

Fig. 4: TEM micrographs of PP/mEPDM/PA6 (70/15/15) reactive ternary blends. (**a,b**) TR1 blend, (**c,d**) TR22 blend. The mEPDM phase was stained by RuO_4

It can be seen that the modifier particles developed an agglomerated structure in the TR1 blend, whereas they form a more or less an interconnected structure of core-shell particles in TR22 blend. These morphological observations from TEM analysis are in agreement with those obtained by SEM analysis made on the etched samples (**Figure 3**).

The schematic representation of the morphologies developed in different PP/mEPDM/PA6 ternary blends is given in **Figure 5**. These schematics reflect the collective observations from many SEM and TEM micrographs. Further details on the development of the different phase morphologies in the reactive ternary blends and the reasons behind are given in the following section (tensile properties).

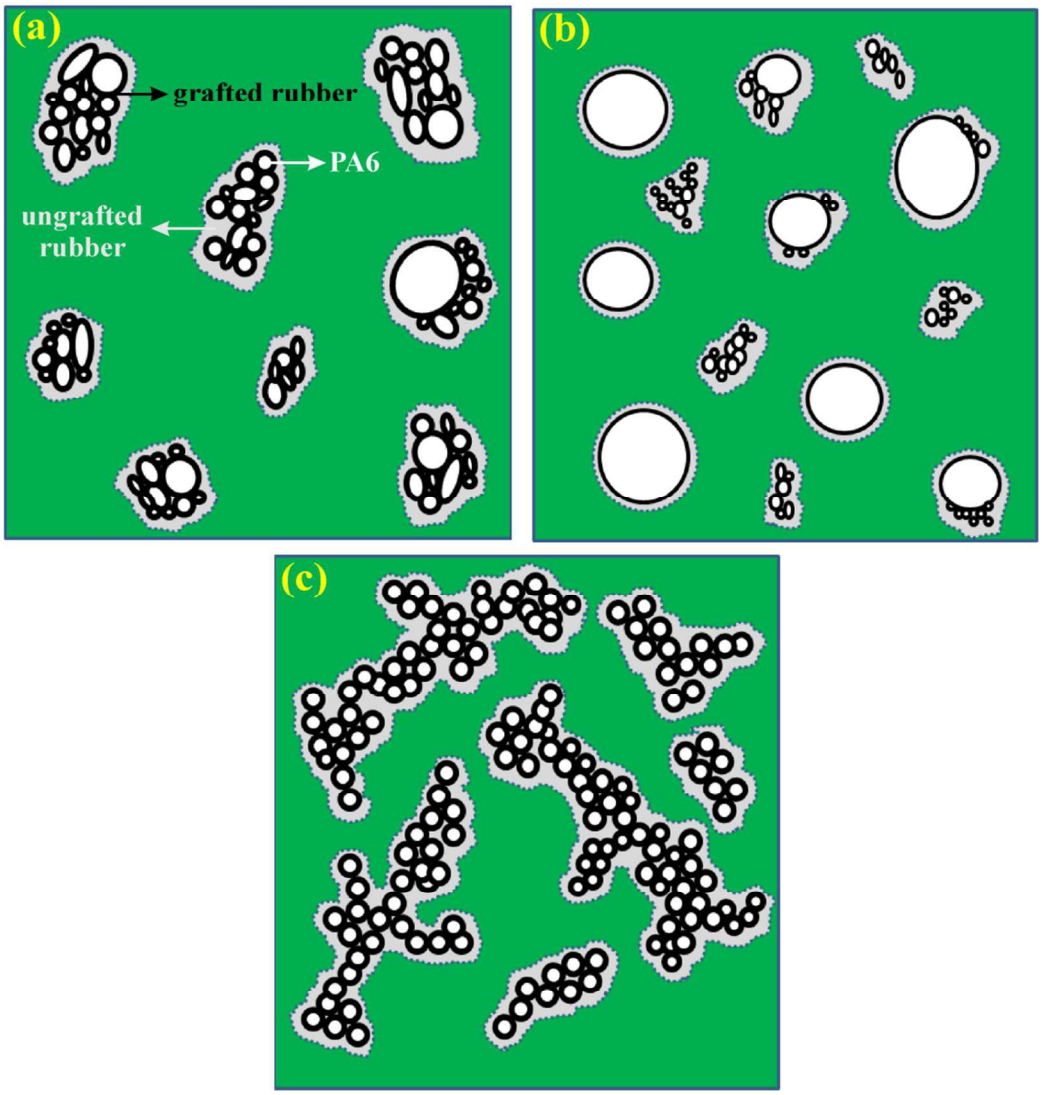

Fig. 5: Schematic illustration of the morphological change in PP/mEPDM/PA6 (70/15/15) reactive ternary blends. (**a**) TR1 blend; (**b**) TR21 blend; (**c**) TR22 blend

Wilkinson et al.[17,18] found that the progressive replacement of SEBS with SEBS-g-MA in PP/PA6/SEBS blends changed the morphology to individual core-shell particles and finally to agglomerates of core-shell particles. In another work, Kim et al.[39,40] reported the formation of agglomerated core-shell particles in PP-based ternary blends. In their work, as the concentration of SEBS-g-MA in the PP/PA6 blend was increased the morphology changed from isolated modifier particles to quasi co-continuous morphology of agglomerated particles.

It has well been documented that the morphology of ternary blends can be predicted through the knowing of interfacial tension values between the components.[8-15] Hobbs et al.[20] used the spreading coefficient concept and rewrote Harkin's equation to predict the morphology of ternary blends, in which two distinct minor phases are dispersed in a major matrix phase. In a ternary blend of three polymers A, B and C (A is the matrix) the spreading coefficient, $\boldsymbol{\lambda_{CB}}$, is defined as:

$$\lambda_{CB} = \alpha_{BA} - \alpha_{CA} - \alpha_{BC} \qquad (5)$$

where $\boldsymbol{\lambda_{ij}}$ is the spreading coefficient of **i** component over **j** component and $\boldsymbol{\alpha_{ij}}$ is the interfacial tension between **i** and **j** components. For B to be encapsulated by C, $\boldsymbol{\lambda_{CB}}$ must be positive. In the case when both $\boldsymbol{\lambda_{CB}}$ and $\boldsymbol{\lambda_{BC}}$ are negative, B and C will tend to form separated phases in A phase.

Here, the morphologies of ternary systems were predicted using the spreading coefficient theory. In this work, the interfacial tension values were calculated based on the surface tension values measured by the contact angle method. The contact angles of PP, PA6, and mEPDM with water and diiodomethane are listed in **Table I**. The surface energy, dispersion and polar components of the materials can be estimated from the contact angle data by using the following two equations (Eq . (5) for water and Eq. (6) for diiodomethane) according to Wu[52]:

$$\left(1 + cos\theta_{H_2O}\right)\gamma_{H_2O} = 4\left(\frac{\gamma^d_{H_2O}\gamma^d}{\gamma^d_{H_2O} + \gamma^d} + \frac{\gamma^p_{H_2O}\gamma^p}{\gamma^p_{H_2O} + \gamma^p}\right) \qquad (6)$$

$$\left(1 + cos\theta_{CH_2I_2}\right)\gamma_{CH_2I_2} = 4\left(\frac{\gamma^d_{CH_2I_2}\gamma^d}{\gamma^d_{CH_2I_2} + \gamma^d} + \frac{\gamma^p_{CH_2I_2}\gamma^p}{\gamma^p_{CH_2I_2} + \gamma^p}\right) \qquad (7)$$

in which $\gamma = \gamma^d + \gamma^p$, γ is surface energy, d is dispersion component and p is polar component, θ_{H_2O} and $\theta_{CH_2I_2}$ are contact angles of the polymer with water and diiodomethane, respectively.

The numerical values used were $\gamma^d_{H_2O} = 22.1\, mN/m$, $\gamma^p_{H_2O} = 50.7\, mN/m$, $\gamma^d_{CH_2I_2} = 44.1\, mN/m$, $\gamma^p_{CH_2I_2} = 6.7\, mN/m$.[52] The values of surface energy, dispersion and polar components of polymers are also listed in **Table I**. Since the melt blending was carried out at essentially higher temperatures, the use of interfacial tension values calculated from surface tension values requires to be extrapolated to the processing temperature, on the basis of data reported for variation of surface tension with temperature (***-dγ/dT***) and polarities (***x_p=γ_p/γ***). Surface tension of mEPDM were determined by means of a simple mixture rule from surface tensions of PE, PP and polyethylidenenorbornene (PENB).[53] The surface tension of PENB was assumed to be the same as that for polybutadiene.[53] Surface tension **γ**, calculated at 230 °C for all the used polymers is listed in **Table I**.

Table I: Contact angle and surface energy values of components.

Sample	Contact angle (°)		Surface tension (mN/m) at 25 °C			Surface tension (mN/m) at 230 °C
	Water	Diiodomethane	Total (γ)	Dispersion component (γ^d)	Polar component (γ^p)	Total (γ)
PP	106.5	66	29.1	28.51	0.59	17.62
PA6	61.3	29.1	51.7	32.94	18.76	38.37
mEPDM	88.8	42.2	39.2	33.26	5.94	27.70

Interfacial tension between polymers was calculated from the well-known harmonic mean equation;[52]

$$\alpha_{AB} = \gamma_A + \gamma_B - \frac{4\gamma^d_A\gamma^d_B}{\gamma^d_A + \gamma^d_B} - \frac{4\gamma^p_A\gamma^p_B}{\gamma^p_A + \gamma^p_B} \qquad (8)$$

The interfacial tension and spreading coefficient values at processing temperature, calculated from the surface tension data, are listed in **Table II**.

Table II: Interfacial tension between the components and spreading coefficient values

Polymer pairs	*Interfacial tension, γ_{ij}(mN/m) at 230 °C*	*Spreading coefficient, λ_{ij}*
PP/PA6	14.1	$\lambda_{AB}<0$
PP/mEPDM	4.2	
PA6/mEPDM	5.3	$\lambda_{BC}<0$, $\lambda_{CB}>0$

A: PP; B: PA6; C: mEPDM

The data demonstrate that in reactive PP/PA6/mEPDM ternary blend, interfacial tension values for PP/PA6 and PA6/mEPDM are higher than that of PP/mEPDM. According to the data outlined in **Table II**, it is clear that the morphology predicted by theoretical calculations is consistent with the real morphologies observed in **Figure 3** for reactive ternary blends. For these blends, the spreading coefficient values in **Table II** suggest complete encapsulation morphology with the mEPDM forming the shell and the PA6 forming the core, which is in accordance with the experimental observation represented in **Figures 3** and **4**. It should be noted that the interfacial tensions of polymer pairs can significantly be changed by *in-situ* reaction at the interfacial region during the reactive blending. Fleischer et al.[54] pointed out that the interfacial tension could be reduced up to 70% through the interfacial modification with an end-functionalized interfacial agent. This means that by considering the chemical reaction of mEPDM with PA6 macromolecular chains during the dynamic melt mixing process, the actual interfacial tension value for PA6/mEPDM pair in the reactive ternary system would be much lower than that reported in **Table II.** A good interfacial adhesion between the PA6 and PP matrix, concluded from SEM images in **Figure 3a-c,** is a consequence of chemical affinity of mEPDM with PA6 phase. The mEPDM localizes at the interfacial region between the PA6 and matrix, and results in a drastic decrease in the interfacial tension between the component pairs. However, as shown in the SEM micrographs of **Figure 3a-c**, the amount of reactive rubbery phase located at the interfacial zone, which subsequently would affect the amount of interfacial tension reduction and the strength of interfacial adhesion, highly depends on the mixing order. This finding further implies that in addition to thermodynamic factors, the kinetic parameters also have a decisive role in the development of phase structure of multiphase blends, especially in reactive systems.

3.2 Relationship between tensile properties and phase morphology

This section elucidates how the different phase morphologies developed in reactive ternary blends affect the macroscopic mechanical behavior of resulting blend under the uniaxial tensile test. The typical stress-strain curves of neat PP, PP/PA6 binary blend and various PP-based ternary blends are displayed in **Figure 6**.

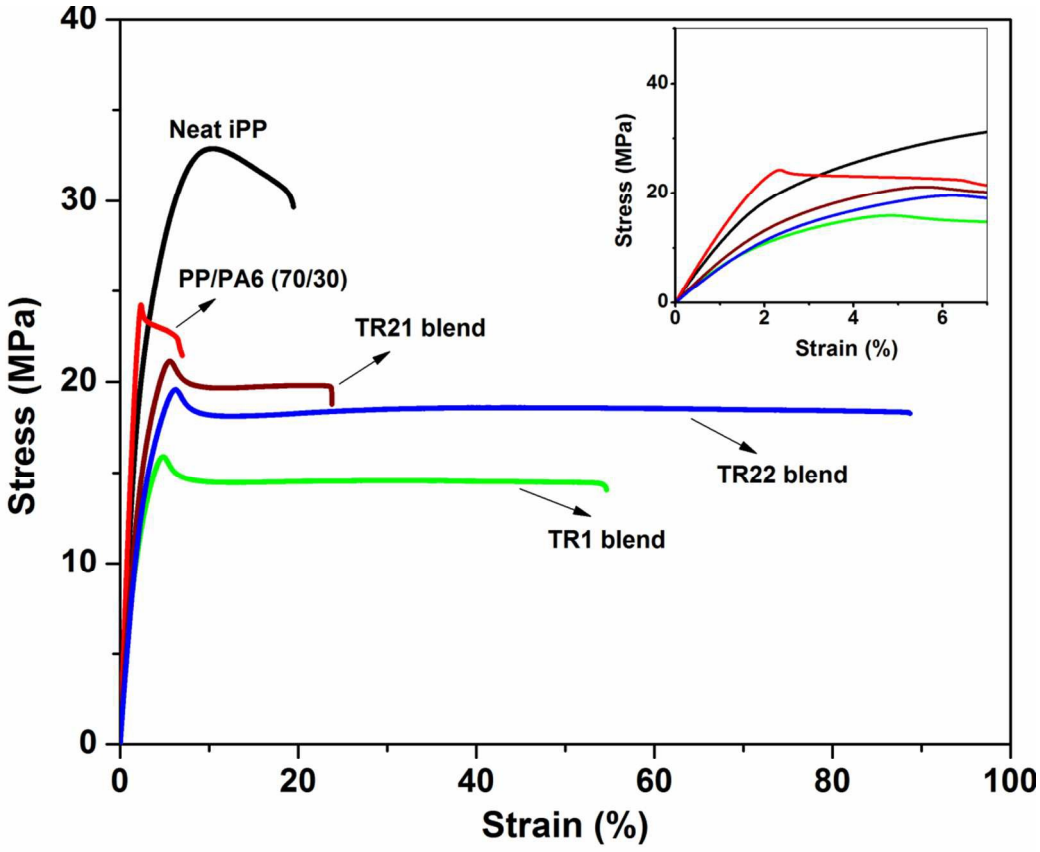

Fig. 6: Tensile stress-strain curves of neat PP, PP/PA6 binary blend, and different PP/mEPDM/PA6 (70/15/15) ternary blends.

As shown in **Figure 6**, the neat PP behaved in semi-ductile manner with completely unstable post-yield deformation behavior, so that the material failed by localized yielding of the tensile bar without the formation of necking zone. PP/PA6 binary blend also showed semi-ductile behavior with much lower yield stress, tensile strength and strain at break values in comparison with pure PP. From **Figure 6**, it is apparent that all the reactive ternary blends show ductile behavior. However, the stress-strain response and, consequently, tensile properties of these blends are strongly dependent on the employed mixing procedure. These different tensile behaviors are a direct consequence of different phase morphologies developed in reactive ternary blends. The Young's modulus, yield stress and tensile strength of the samples are depicted in **Figure 7.**

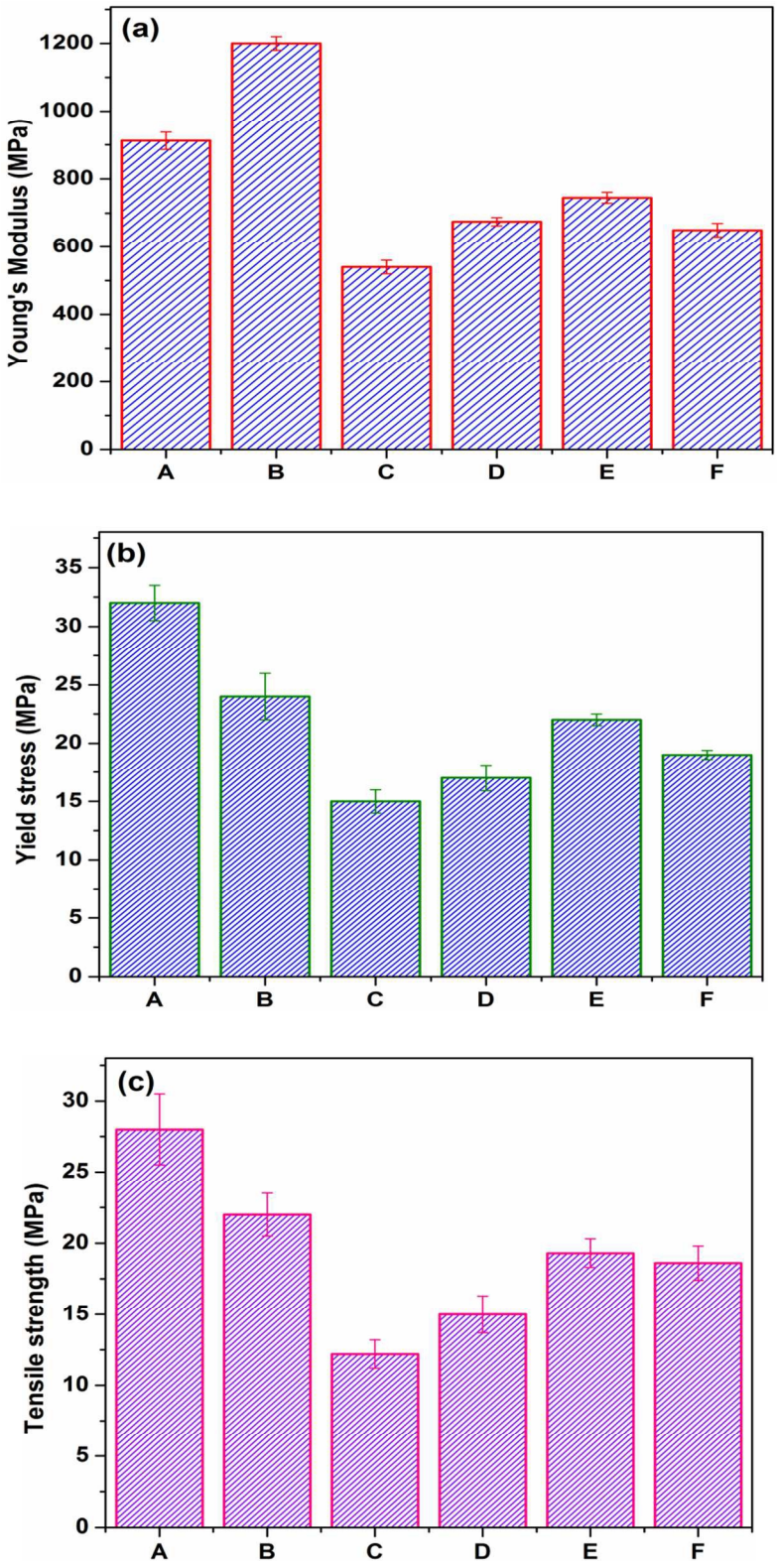

Fig. 7: Tensile properties of different samples. (**a**) Young's Modulus, (**b**) yield stress, and (**c**) tensile strength. (**A**) neat iPP; (**B**) PP/PA6 (70/30); (**C**) PP/mEPDM (70/30); (**D**) TR1 blend; (**E**) TR21 blend; (**F**) TR22 blend.

In comparison with pure PP, the PP/PA6 binary blend showed larger Young's modulus along with much lower yield stress and ultimate strength. By considering that the PA6 has higher Young's modulus ($\approx 1.9\ GPa$), yield stress ($\approx 74\ MPa$) and ultimate strength ($\approx 50\ MPa$) than the pure PP, higher elastic modulus of PP/PA6 blend could be attributed to the presence of PA6 phase with larger stiffness than the pure PP, while the reduction of yield and tensile strength values could primarily be related to poor interfacial bonding between the components in this binary blend. The latter statement was evidenced by the SEM micrograph of phase morphology presented in **Figure 1a**. The expected great decrease in Young's modulus, yield stress and tensile strength parameters for PP/mEPDM binary blend, as compared with those for pure PP, arises mainly from the presence of soft rubber particles in the binary system which reduces the stiffness and strength of the resulting material.

In the case of ternary blends, the data demonstrate that all the reactive ternary systems have tensile moduli values lower than those for pure PP and PP/PA6 binary blend, while larger than that of PP/mEPDM binary blend. In addition, different elastic moduli were obtained for ternary systems, depending on the mixing procedure. As can be seen, the TR21 blend shows the largest whereas the TR22 blend displayed the lowest value of tensile modulus. In the case of TR21 reactive ternary blend, it should be noted that the reactive rubbery phase (mEPDM) is melt mixed with PA6 phase at the first stage of the blending process. Therefore, the grafting of PA6 macromolecular chains onto the functionalized rubber chains not only compatibilizes the rubbery phase with the PA6 polymer but also causes a significant increase in the molecular weight and melt viscosity of the system. These processes highly reduce the propensity of rubbery phase for diffusion into the interfacial region (as an interfacial agent) or even its subsequent localization within PP matrix (as a toughening agent) during the second step of blend preparation. The result is that larger PA6 droplets are formed in the ternary system and the stress-strain behavior of the material becomes close to that of PP/PA6 binary blend (**Figure 6**). In the case of TR22 reactive ternary blend, in which the reactive rubbery phase was firstly melt mixed with PP and the resulting blend was incorporated by PA6 phase, a fine and uniform distribution of mEPDM particles throughout the PP matrix is developed during the first step of blend preparation. Upon the incorporation of PA6 phase into compatible PP/mEPDM blend, the finely dispersed rubber particles effectively improve the dispersion of PA6 phase domains within the matrix owing to their strong chemical affinity towards PA6 phase, which subsequently form an interfacial layer

between PA6 phase and PP matrix. Consequently, a much more efficient performance of the rubbery phase as a compatibilizing agent (interfacial modifier) is achieved in the TR22 system as compared with other reactive blends. This statement was confirmed by comparison of phase morphology of different reactive blends as represented in **Figures 2-4**. For this reason, this system represents the smallest Young's modulus among the ternary systems. The reactive ternary blend of one-step mixing which is composed of both relatively large PA6 domains and dispersed clusters of core-shell particles has an intermediated elastic modulus. Since the PA6 and mEPDM components are simultaneously introduced into the mixing chamber, it is believed that the fast and high reactivity of functionalized rubbery phase towards PA6 phase during the initial stages of blending prevents to some extent the rubbery phase from being homogeneously distributed within the matrix and/or uniformly encapsulate the PA6 dispersed domains. This would result in the formation of relatively large island-like clusters in the matrix.

The data in **Figure 7b,c** reveal that there is a significant difference in yield stress and tensile strength of reactive ternary systems prepared in different methods. The TR21 ternary blend exhibits the maximum values of yield and tensile strengths while the minimum values are related to the TR1 ternary blend. According to the descriptions made earlier in the case of elastic modulus, the former observation can be ascribed to the presence of a small fraction of rubbery phase at the interfacial region and/or within the matrix phase of TR21 blend. It is well established that the factors like phase morphology (dispersion state) and dispersed domains/matrix interfacial strength substantially affect the yield stress and tensile strength of polymer blends.[55,56] In fact, the strength of multiphase systems is determined by the extreme values of such parameters as the interface adhesion, stress concentration and defect size/spatial distribution.[55] Therefore, it can be concluded that in reactive ternary blends, a larger and more intense stress concentration on the relatively large discrete clusters of agglomerated core-shell particles in TR1 blend, as compared with the TR22 blend, facilitate early debonding and/or interfacial void formation at the interface of island-like domains and the matrix, and this is responsible for low value of yield stress in this system. The higher interfacial adhesion between the components in the TR22 ternary blend together with finer and more uniform distribution of core-shell particles not only increase the yield stress and ultimate strength of the material but also participates larger volume of material in the energy absorption processes, which in turn improves the tensile ductility of the blend.

The elongation at break values for neat PP, binary and ternary blends are represented in **Figure 8**. As can be seen, the PP/mEPDM binary blend exhibits the highest elongation at break among the samples studied in this work. The significantly higher elongation at break value of PP/mEPDM binary blend in comparison to other samples comes from the rubber-toughening effect of dispersed rubber particles. The smaller tensile ductility of ternary blends than the rubber-toughened binary blend could be attributed to the lower volume fraction of soft rubber particles in the former blends. Similar to other tensile properties, the elongation at break of reactive ternary blends also depends strongly on the procedure of blend preparation. It is reasonable to observe that the reactive ternary blend that contains homogeneous distribution of core-shell particles shows much higher post-yield deformation stability (tensile strain) owing to the delocalized (more homogeneous) deformation processes in the material induced by percolated core-shell particles. As a consequence of low rubber content localized in the interfacial region and/or in the matrix, the TR21 blend shows the lowest tensile ductility among the different ternary blends. It is believed that the concentration of rubbery phase mostly around and/or within the island-like structures in the TR1 blend makes the rubbery phase ineffective in improving the tensile ductility of the ternary blend under the uniaxial tensile test as compared with the TR22 blend.

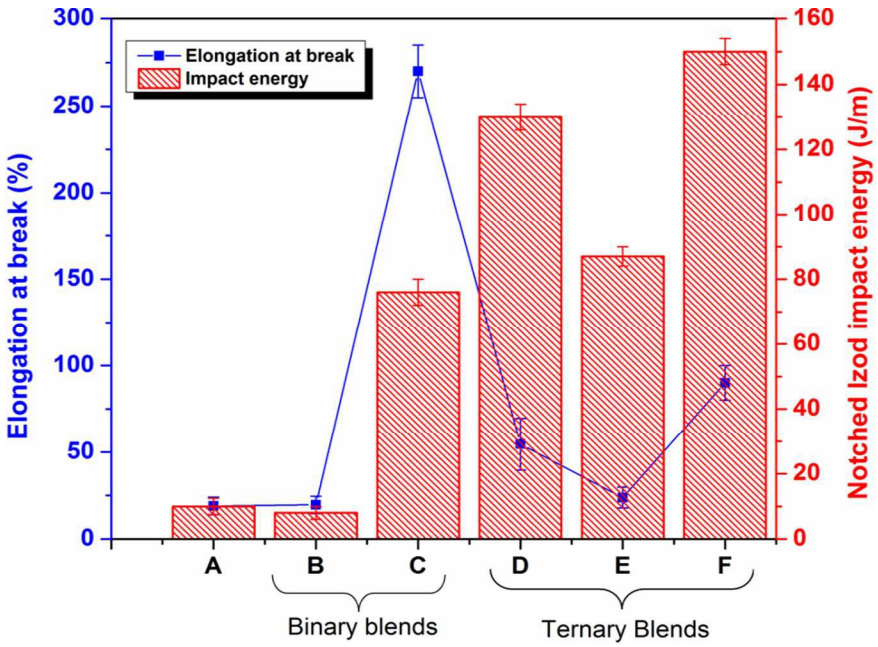

Fig. 8: Elongation at break and notched Izod impact strength of different samples.(**A**) neat iPP; (**B**) PP/PA6 (70/30); (**C**) PP/mEPDM (70/30); (**D**) TR1 blend; (**E**) TR21blend; (**F**) TR22 blend.

3.3 Relationship between Izod impact toughness and phase morphology

PP, PA6 and their blends are widely used in automobile and construction industry due to their balanced mechanical properties. However, their application is restricted owing to their notch-sensitive property and brittleness under triaxial and/or impact loadings, especially at low temperatures. Therefore, the improvement of their impact resistance is of great importance. The notched Izod impact strength of different samples is shown in **Figure 8**. Compared to neat PP, binary PP/PA6 blend showed lower impact strength value, as expected. The incorporation of mEPDM rubbery phase into pure PP caused a remarkable improvement in the impact resistance of the material, also as expected. However, the improved impact strength and tensile ductility of rubber toughened binary PP/mEPDM blend is at a cost of a great reduction in other engineering properties such as stiffness and ultimate strength (**Figure7**). For this reason, attempts are made in different research works to overcome the deficiency related to the use of rubbery phase by using a rigid polymeric phase such as PA6 to obtain a multiphase material with balanced toughness and stiffness. It is very interesting to observe that the Izod impact toughness of reactive PP/PA6/mEPDM (70/15/15) ternary blends is significantly enhanced compared to the toughened PP/mEPDM binary blend. This finding is very important because the improved impact strength of the reactive ternary blends is achieved at much lower rubber content as compared to PP/mEPDM binary blend. As can be seen, the extent of improvement in the impact toughness value is highly dependent on the order of mixing of blend constituents. The lowest enhancement is for TR21 blend, whereas the greatest increase was found for TR22 sample. The TR1 sample showed remarkably higher impact strength than the TR21, but lower than the TR22 system. Although both the TR1 and TR22 blend systems displayed highly-toughened multiphase blends, the impact data indicate that the development of a percolated structure of core-shell particles is more effective than the discrete clusters of core-shell particles in energy dissipation under the impact loading. This observation further highlights the importance of the dispersion state of the modifier particles in enhancing the impact strength of the multiphase systems. In this study almost 15 times' increase in Izod impact toughness was achieved for PP at a low content of rubbery phase. This is an excellent increase in the impact strength, which was achieved in TR22 reactive system. The impact energy for TR1 and TR21 blends was, respectively, about 13 and 8.7 fold greater than that of neat PP. It is worth noting that the extent of improvement obtained in PP-based ternary blends in this work is higher than those reported in the literature for PP blends

toughened by other rubbery phases at the same dispersed phase composition, [17, 18, 50,51] though in the work by shokoohi et al.[50,51] the authors did not elucidate the amount of improvement in the mechanical properties at optimum condition over those for neat PP matrix. A comparison between the impact data of reactive ternary blends (especially TR1 and TR22 samples) and toughened binary blends in this work reveals that the dispersed phase morphologies with agglomerated and/or percolation of core-shell structures are much more efficient in the absorption/dissipation of impact loadings than the dispersed individual domains of rubber particles in PP/mEPDM binary blend, even at much lower rubber loadings. Although the TR21 reactive system showed significantly lower impact strength value than the other reactive blends, its impact toughness is still higher than the toughened binary blends, probably due to the presence of small aggregates of dispersed modifier particles in this system. The toughening micro-mechanisms responsible for the high impact toughness obtained in reactive ternary blends will be discussed in the following sections.

It is worth noting that the impact strength of the samples did not follow exactly the same trend as the elongation at break (**Figure 8**). The results **in Figure 8** demonstrate that the toughness in terms of material's extensibility under uniaxial tensile loading, which is usually performed at a constant low-strain rate condition, is more dependent on the content of rubbery phase compared with the toughness in terms of impact energy under the notched Izod impact loading which is carried out at substantially high speeds.

3.4 Phase compatibility of the blends

Phase morphology as a determining factor for properties of multicomponent polymer systems, is controlled by the interfacial interactions and compatibility of the blends' components. In the present work, the dynamic mechanical properties of the studied blends were examined to further substantiate the understanding from the microstructure of complex systems consisting of three phases. The storage modulus (G') and damping factor ($\tan\delta$) curves of neat PP and PP-based ternary blends are shown in **Figure 9a,b**.

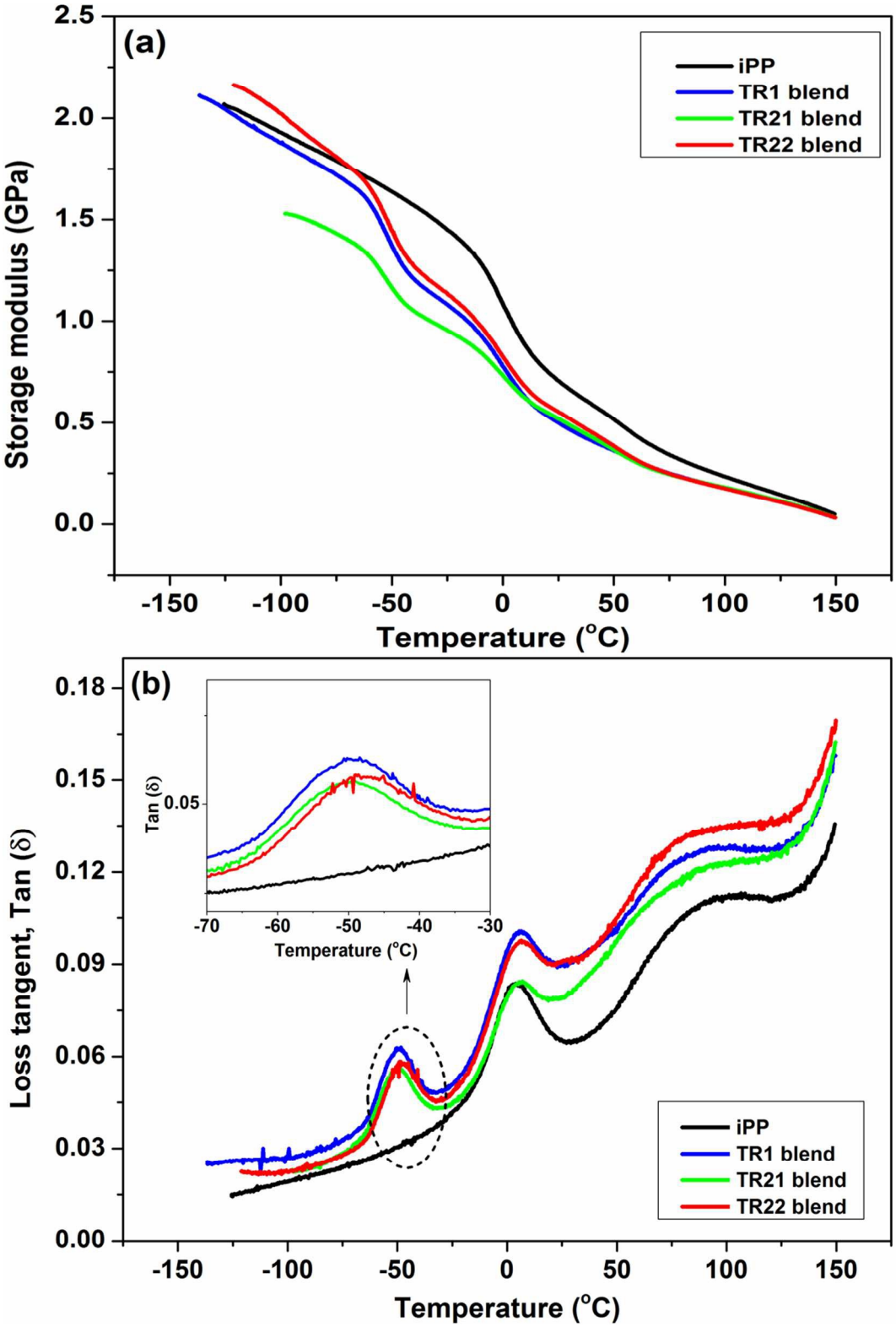

Fig. 9: DMA traces of neat iPP and different PP/mEPDM/PA6 (70/15/15) reactive blends. (**a**) storage modulus versus temperature; (**b**) tan δ versus temperature curves.

The storage modulus is directly related to the elastic response of the tested material, whereas tan δ is intimately associated with the chain relaxation that takes place. From **Figure 9a**, it is apparent that all the curves experience a gradual decline in G' with increase in temperature from -140 ℃ to 150 ℃, as expected. They show two or more transitions in G' during the heating cycle, which are indicative of immiscibility of the different polymeric components. In addition, the ternary blends exhibit lower storage modulus as compared with the pure PP, most probably due to the presence of rubbery phase. The plot of tan δ reveals more clearly the corresponding transition temperatures and the breadth of transition zone, **(Figure 9b)**. Two distinct transition peaks were recorded for neat PP, one at about 4.5 ℃ that corresponds to the β-transition and the other at about 105 ℃ representing the α-relaxation.Reactive ternary blends showed higher tan δ values in comparison with pure PP, which can be attributed to rubbery phase present in the ternary systems. With the ternary blends, the first set of distinct transition peaks at low temperatures (inset in **Figure 9b**) arises from the relaxation of rubbery phase in the ternary systems. The second peaks are associated with the β-relaxation of PP phase as the matrix material. The third transition peaks are related to the relaxation of PA6 phase and α-relaxation of PP phase, which are superimposed. The most striking observation in **Figure 9b** seems to be the transition related to the rubbery phase. It is clearly apparent that the shape, intensity and the location of rubbery phase transition peak are markedly affected by the blending sequences. The TR21 blend displays the least rubbery phase transition along with relatively broader third (high temperature) transition in comparison with other blends. The former observation indicates to a comparatively small segregated volume of mEPDM available in the matrix to undergo glassy transition and the latter result implies the presence of grafted rubbery chains in the PA6 phase domains which produce more heterogeneity in the polar phase leading to broadened relaxation. In contrast, the TR1 reactive blend shows the most dramatic transition owing to the segregated rubbery phase around and/or inside island-like micro-clusters, which reflects the large phase volume of mEPDM that undergoes an intense glassy transition. For the TR22 reactive blend, peak intensity is remarkably less than that for TR1 blend. Moreover, it seems that the peak temperature is slightly shifted to higher temperatures. This result suggests a less segregated rubbery phase in the blend especially within the aggregated core-shell domains in the TR22 ternary system, reflecting that a finer and better distribution of the rubbery phase is obtained. Since the rubbery phase serves as both the compatibilizing agent and toughener in the ternary

blend, it can be concluded that a highly improved distribution of core-shell particles would developed in the TR22 reactive blend as compared with other reactive systems. By considering the fact that in dynamic mechanical analysis the loss tangent parameter is a measure of material's capability for energy dissipation processes, it is very interesting to observe that the toughness of ternary blends as measured by notched impact testing at ambient temperature (**Figure 8**) follows the same trend as that determined by loss tangent data at room temperature (**Figure 9b**), i.e., TR22 blend ≈ TR1 blend >> TR21 blend.

3.5 Thermal and crystallization behaviors

Based on the fact that PP is a semicrystalline polymer, it is expected that the mechanical properties of PP matrix ternary blends prepared in this work would be influenced by the matrix crystallinity. Therefore, the study on the crystalline structure of the blend systems prepared in this work is of great importance to determine the possible alteration in the matrix crystallinity in reactive blends and its subsequent effect on the impact toughness. The melting and crystallization behavior of neat phases and different ternary blends are given in **Figure 10**. The results from DSC thermal scans are summarized in **Table III**.

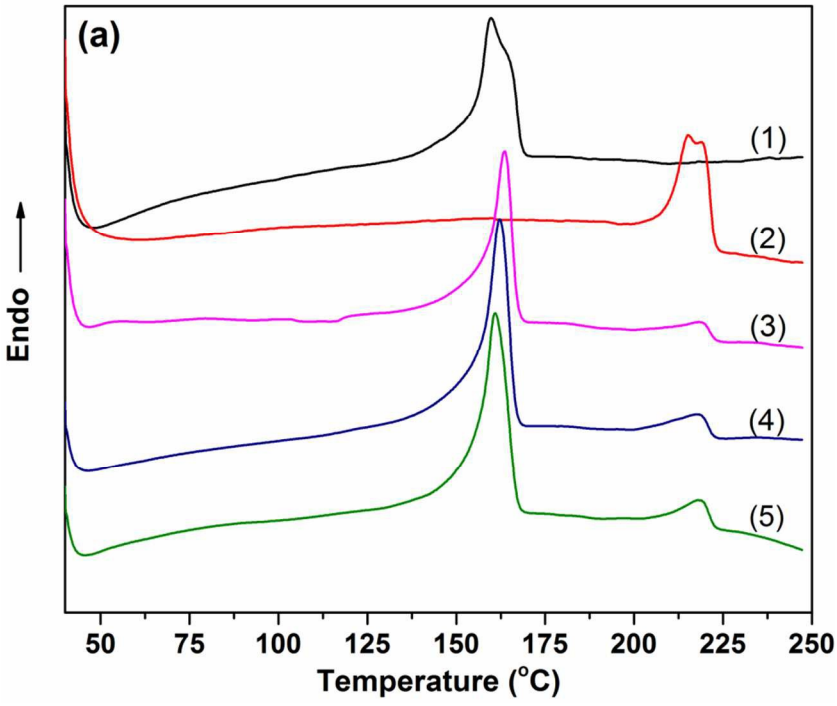

Fig. 10: DSC results for neat polymers and different blend systems. (**a**) heating curves, and (**b**) cooling curves. (1) neat PP, (2) neat PA6, (3) TR1 blend, (4) TR21 blend, (5) TR22 blend.

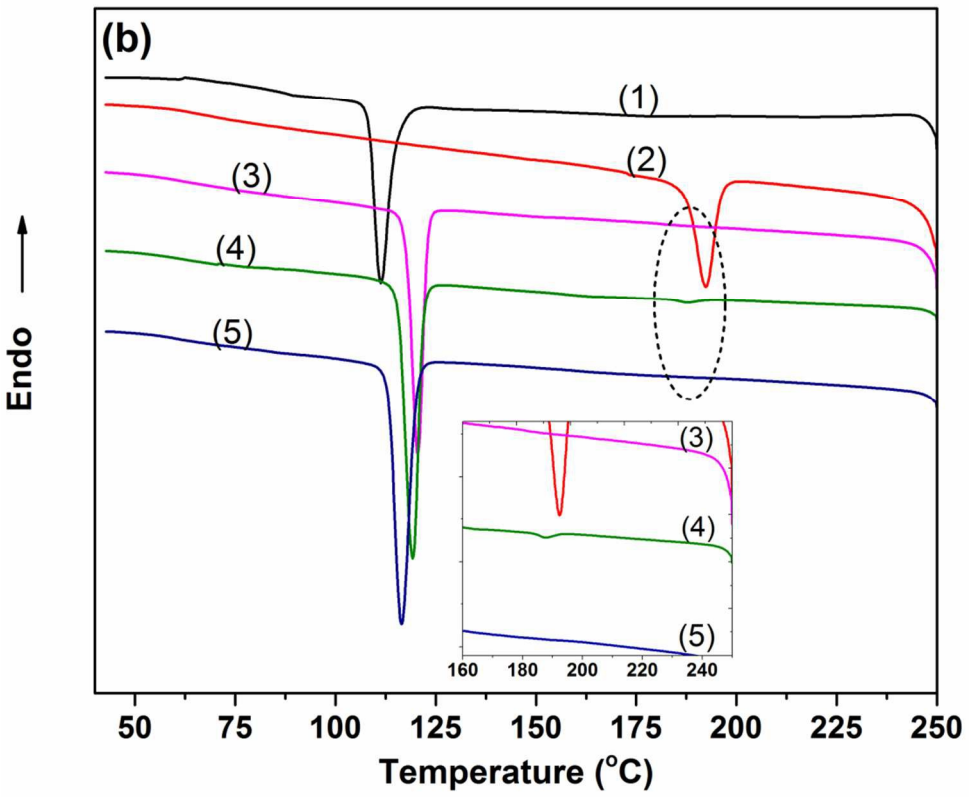

Fig. 10: Continued from previous page

Table III: Thermal properties of neat polymers and ternary blends.

Samples	$T_{c,PP}$(℃)	$T_{m,PP}$ (℃)	$\Delta H_{c,PP}\ (J/g)$	$\Delta H_{m,PP}\ (J/g)$	$X_{c,PP}$ (%)	$T_{c,PA6}$ (℃)	$T_{m,PA6}$ (℃)
PP	111.35	159.7	96.88	94.93	45.2	-	-
PA6	-	-	-	-	-	193.3	213, 218
TR1	120.58	163.55	71.00	54.97	37.5	-	216
TR21	119.28	162.70	77.66	63.67	43.5	191	216
TR22	116.44	160.84	81.60	67.95	46.4	-	216

According to **Figure 10** and **Table III**, the crystallization peak temperature of the PP in the ternary blends is significantly increased compared with that of neat PP. This is because the solidification of PA6 particles dispersed in the PP melt results in heterogeneous nucleation of the PP. As can be seen, the TR22 sample shows the lowest crystallization peak temperature of the PP among the reactive ternary systems, reflecting the more perfect and better encapsulation of PA6 particles by the mEPDM in this reactive system compared to other reactive blends. The significant change in the thermal behavior of reactive ternary blends (especially for TR1 and

TR22 samples) is the disappearance of the crystallization exotherm at approximately 193 °C related to PA6 homopolymer crystallization (**Figure 10b**). This change could be attributed to the fractionated crystallization of PA6 phase, since engulfed and finely dispersed PA6 particles in the reactive ternary blends could not effectively serve as heterogeneous nuclei typical of the bulk PA6.[18, 47] The data in **Table III** further demonstrate that the degree of crystallinity of PP matrix in different reactive ternary blends (which exhibited greatly improved impact strength) does not change significantly as compared with that of neat PP. Although a decrease in the degree of crystallinity of PP matrix was observed for TR1 blend, this could not be responsible for a remarked increase in the impact strength of the resulting blend. This statement is further confirmed by the fact that the TR22 blend with the highest degree of crystallinity among the samples studied (and therefore higher matrix crystallinity than the TR1 blend), exhibited the greatest impact toughness. From the results of thermal studies in conjunction with those of impact strength it is concluded that the tremendous improvement achieved in impact toughness of TR1 and TR22 reactive ternary blends is mainly due to the development of unique phase morphologies in these systems and not as a result of alteration of crystallization behavior.

3.6 Impact-Fractured surface analysis of the blends

To further study the toughening effect in binary and ternary blends, the impact fractured surface of the specimens was investigated by SEM and the micrographs are shown in **Figures 11** and **12**. All the micrographs in these figures correspond to the back of crack-initiation region. **Figure 11** shows the impact fractured surfaces of pure PP and different PP-based binary blends. The neat PP showed a smooth and featureless fracture surface with no sign of much deformation, indicating a typical brittle mode of failure. The fracture surface of PP/PA6 (70/30) blend is also relatively smooth. Due to poor interfacial adhesion between the PP and PA6, the dispersed PA6 domains debonded and/or pulled out from the surrounding matrix under the impact loading. This would lead to the formation of large micro-voids/micro-cracks in the material, which is responsible for lower impact strength of PP/PA6 blend than the neat PP. All the other blend systems studied in this work exhibited distinct stress whitening around the fracture plane of impact specimens, the extent of which was dependent on the composition and phase structure of the material.

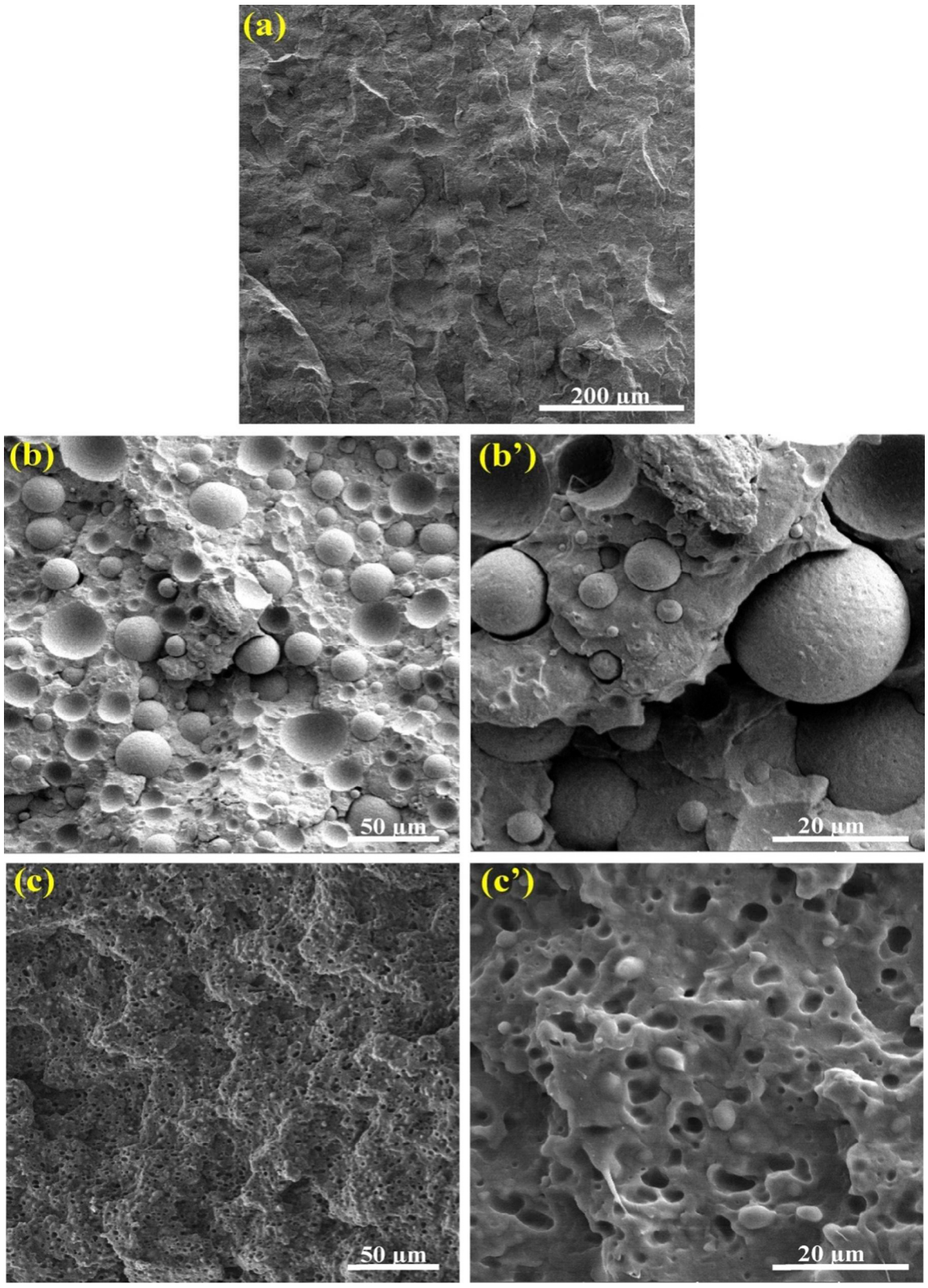

Fig. 11: SEM micrographs of impact-fractured surfaces of neat PP and binary blends. (**a**) neat iPP; (**b,b'**) PP/PA6 (70/30); (**c,c'**) PP/mEPDM (70/30).

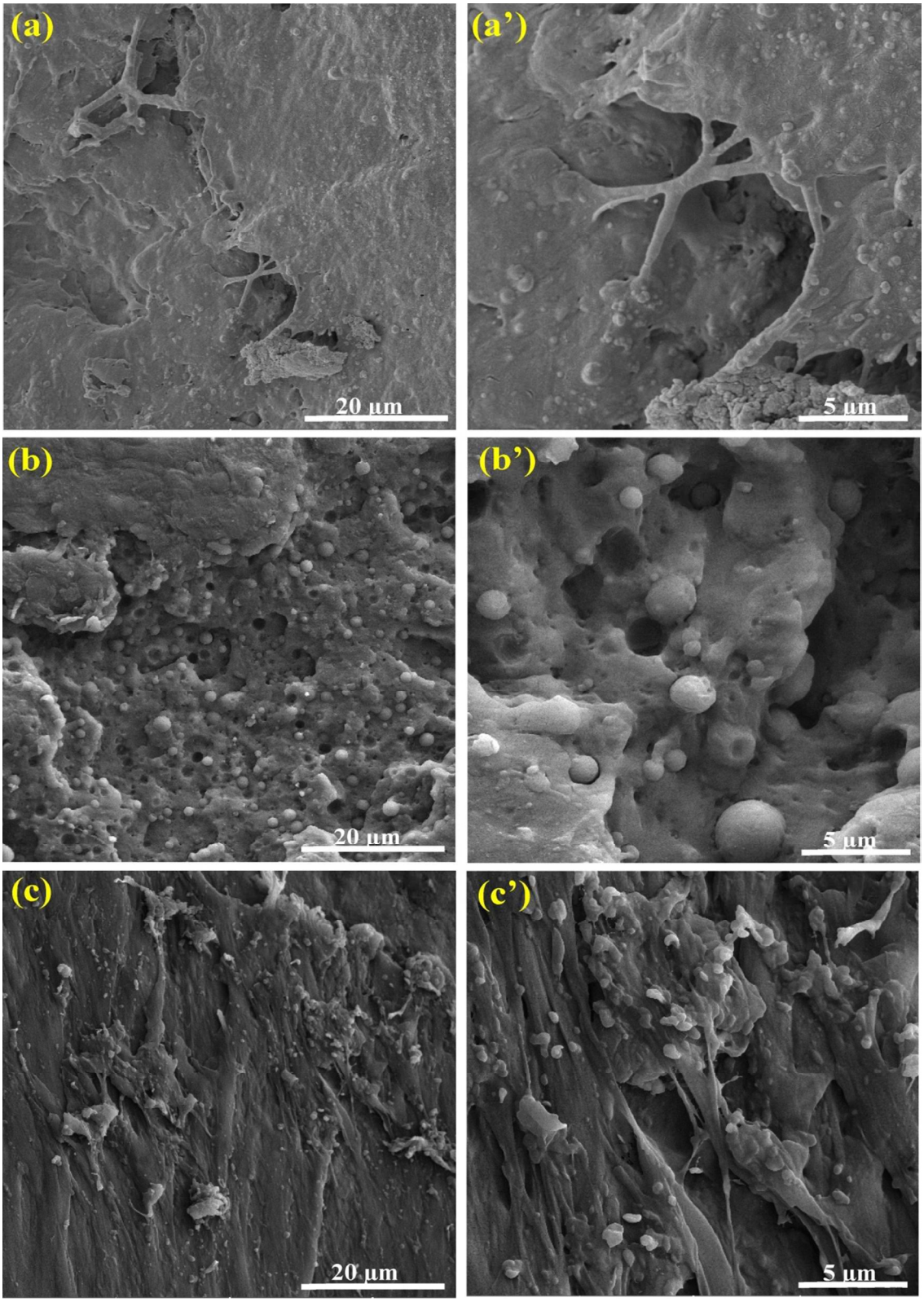

Fig. 12: SEM micrographs of impact-fractured surfaces of reactive PP/mEPDM/PA6 (70/15/15) ternary blends. (**a,a'**) TR1 blend; (**b,b'**) TR21 blend; (**c,c'**) TR22 blend.

In comparison to PP/PA6 binary blend, the fracture surfaces of PP/mEPDM (70/30) blend showed increased roughness, and some signs of plastic deformation were discernible on the fractured surface. As can be seen, there are a large number of cavities appeared on the fractured surface of PP/mEPDM binary blend. These voids come mainly from the cavitation of dispersed rubber particles, although some debonding and/or rupturing of the rubber particles may also contribute to the void formation. It is well documented that the cavitation of rubber particles relieves the triaxial stress states on the rubber particles and, thereby, plays an essential role on the toughening effect.[57-59] By suppressing locally the triaxial stress, the stress distribution around the particle equator becomes more favorable to the initiation of shear yielding process of the matrix.[57-59] Moreover, the fracture surface of PP/mEPDM binary blend represents a considerable number of mEPDM rubber particles which are strongly adhered to the surrounding matrix phase without debonding and/or internal cavitation. These processes are responsible for much higher impact strength of PP/mEPDM blend than those for PP and PP/PA6.

For TR1 ternary blend, the micrographs in **Figure 12a,a'** revealed a homogeneous shear yielding of the matrix material. High magnification micrograph shows that the matrix material around and in-between the dispersed structures are strongly yielded and plastically deformed. The destruction of the agglomerated structures as a result of plastic flow of the matrix material is also clearly visible in the micrograph. Some cavities are also visible on the fracture surface of this sample. These cavities could be formed by micro-voiding of rubbery phase encapsulated PA6 particles within the agglomerated structures and/or in the layer between the agglomerates and the matrix. It is believed that the nucleation, development and plastic growth of these micro-voids play an essential role in improving the impact toughness of the material. In contrast with the TR1 sample, the impact-fractured surface of TR21 sample showed less intense shear yielding of the matrix, suggesting lower energy dissipated during the crack growth. As a result, the impact resistance of this sample would be lower than that of TR1 blend. The dispersed modifier particles which are discretely distributed and partly bonded to the surrounding matrix material are apparent on the fracture surface. Moreover, there are numerous cavities on the fracture surface in the form of isolated cavities with relatively large size (in the order of dispersed domains), interfacial voids at the interface between the dispersed PA6 domains and the matrix, and tiny cavities randomly distributed throughout the deformed surface. By considering the fact that the modifier particles in TR21 blend are consisted of individual core-shell PA6/mEPDM particles,

the appearance of interfacial voids could be related to the cavitation of the thin rubbery shell surrounding the PA6 particles. Since the impact strength of TR21 sample is even greater than that of PP/mEPDM binary blend, it is concluded that the combined presence of composite dispersed droplets with a relatively thin layer of interfacial rubbery phase and small aggregates of modifier particles is more efficient in the dissipation of impact loadings than the conventional homogeneous dispersed domains of rubbery phase. For TR22 ternary blend, a homogeneous shear yielding and plastic deformation is clearly visible on the fracture surface. As can be seen, however, the morphology and texture of fractured surface for TR22 sample is different from that of TR1 and TR21 blends. In fact, more intense plastic deformation appear on the fracture surface of TR22 sample compared to other blends, and there is also some evidence of the formation of bands consisting of highly deformed matrix material. This indicates that much more fracture energy is dissipated via the above-mentioned micromechanical deformations during the impact fracture of TR22 sample, and this is consistent with its higher impact strength than the other reactive blends studied in this work. The intensive plastic flow of matrix material around and in-between the large dispersed structures in the form of highly elongated bands justify the excellent impact toughness of TR22 blend. As a result of good interfacial adhesion between the dispersed agglomerates and the matrix, a severe deformation/disintegration of dispersed structures during the plastic deformation of the matrix could also be seen in the micrograph.

3.7 Toughening mechanisms

It is well-established that the toughening mechanisms involved in different blend systems are influenced strongly by the phase structure of various modifier particles, which in turn leads to different micromechanical deformations. This is because the morphology of different types of modifier particles greatly affects the local stress fields, which play the major role in activation of different energy-absorbing micro-mechanisms. It is commonly accepted that the modifier particles act as stress concentrators under external loadings, and alter the stress state in the polymer matrix around the particles via internal cavitation or debonding. To achieve high toughening effect, the dispersed particles should have suitable interfacial adhesion with the matrix to improve the dispersion state and also to inhibit micro-crack formation. Poor interfacial adhesion will produce phase segregation and cannot afford the crack formation. As discussed above, in this work the TR22 sample with a unique phase structure compared to the other

samples showed superior impact strength. To establish the toughening mechanisms of the blends, the impact fractured morphologies of reactive ternary blends was further characterized using SEM, and are shown in **Figure 13**.

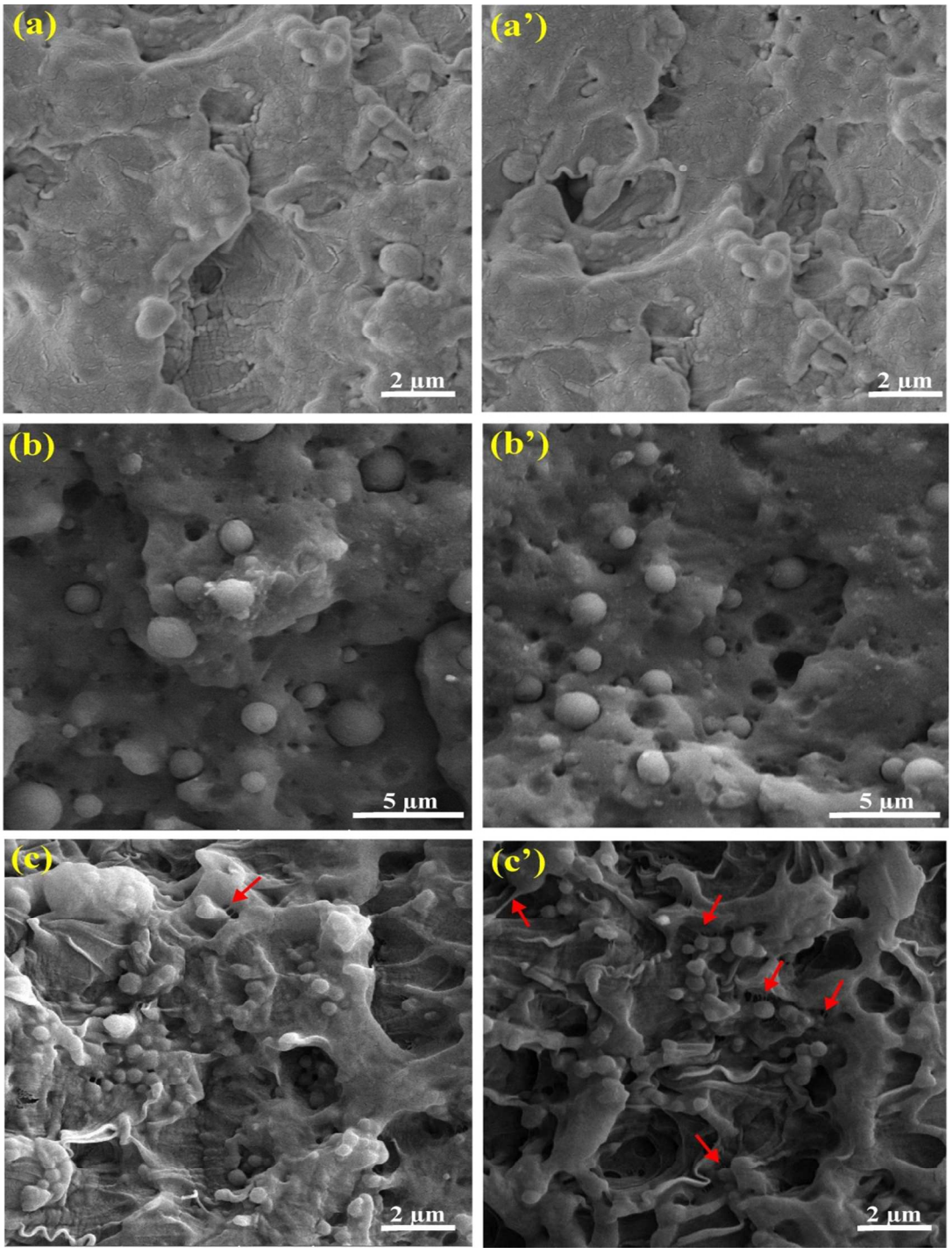

Fig. 13: SEM micrographs of impact-fractured surfaces of reactive PP/mEPDM/PA6 (70/15/15) ternary blends. (**a,a'**) TR1 blend; (**b,b'**) TR21 blend; (**c,c'**) TR22 blend.

For TR1 sample, the micrographs reveal micro-void formation and shear yielding of the matrix material. It is obvious that the void formation occur within the dispersed agglomerates or at the interface of agglomerates and PP matrix, though a good bonding between the dispersed structures and the matrix is apparent. This type of void formation could be attributed to the cavitation/debonding of rubbery phase either as a shell around the PA6 particles inside the clusters or as an interfacial layer between the dispersed clusters and the matrix. The matrix around the agglomerated structures has been yielded and plastically deformed. The same micromechanical deformations are also operative in TR21 blend, but with intensities different from those in TR1 sample. Compared to the TR1 blend, matrix shear yielding is much less intense, whereas the extent of interfacial voiding and debonding is much more significant in TR21 sample. There is evidence of some interfacial bonding between the dispersed modifier particles and matrix, suggesting that a relatively thin layer of the shell forming rubbery phase presents at the interfacial region. The relatively poor interfacial adhesion between the modifier particles and the matrix promotes crack formation during the impact loading, which results in very limited improvement in the toughness. However, a different deformation phenomenon was observed for TR22 blend. Massive shear yielding and plastic deformation of the matrix is clearly visible in the micrographs. There is also evidence of debonding or void formation (in some cases fibrillated voids as indicated by arrows in **Figure 13 c,c'**) either inside the dispersed structures or at the interface between the modifier particles and the matrix. It seems that these voids have plastically grown and elongated as a result of severe plastic flow of the surrounding matrix material. It can be seen that although some interfacial voids have been formed, the interfacial adhesion of dispersed structures with the matrix is strong enough to inhibit crack formation. This different deformation process resulted in different toughness properties and tremendously enhanced impact strength. The results also indicate that the finer and more homogeneous dispersion of core-shell particles in the form of interconnected phase morphology is much more efficient in activation of extensive shear yielding of the matrix material in comparison with other dispersed phase structures. This finding is in agreement with the results reported in the literature for other multiphase systems.[17,18,41-43] According to the SEM observations in **Figure 12 c,c'** it can be concluded that the percolated morphology could enable the deformation bands to grow and thus consumes more energy before fracture. It is worth noting that the improved in fracture energy may also be due to crack deflection around the dispersed structures. The discrete clusters

or extended structures, in TR1 and TR22 blends respectively, could increase the impact toughness via preventing the crack propagation through the material. This latter statement will be verified and discussed in more detail in our next work which evaluates the fracture resistance of the ternary blends presented above via a fracture mechanics-based approach.

The micromechanical deformation processes responsible for improved impact strength of ternary blends studied in this work could be elucidated by the micromechanical model proposed by Kim et al.[41,42] In the case of TR1 and TR22 samples, studied in this work, the deformation sequences are consisted of the following stages; 1) stress concentration around the agglomerated or interconnected structures, 2) deformation of dispersed structures followed by multiple micro-void formation in the rubbery layer both between the PA6 particles within these structures and in the layers between them and the matrix, and 3) relieving the concentrated triaxial stress fields followed by the activation of shear yielding process in the matrix ligament around and in-between the dispersed structures. Moreover, it should be noted that overlapping of stress fields around the dispersed structures along with the crack deflection effects become progressively more pronounced as the dispersion state of modifier particles transforms into larger agglomerates and finally to percolated structures. The more continuous stress fields throughout the matrix material with higher intensity as a result of overlapping of stress fields, not only facilitates and, thereby, intensifies the shear yielding and plastic deformation of matrix material but also participates the much larger volume of the material in different energy absorption/dissipation processes. As a result, the impact fracture toughness of the material is greatly improved. Consequently, the percolated structure (RT22 sample in this work) generate more extensive shear yielding of the matrix than the discrete clusters of modifier particles (RT1 sample in this work), and the discrete clusters still show greater plastic flow as compared with the individual core-shell particles (TR21 sample in this work). According to these explanations, a schematic representation showing the toughening mechanisms for different morphologies is depicted in **Figure 14**.

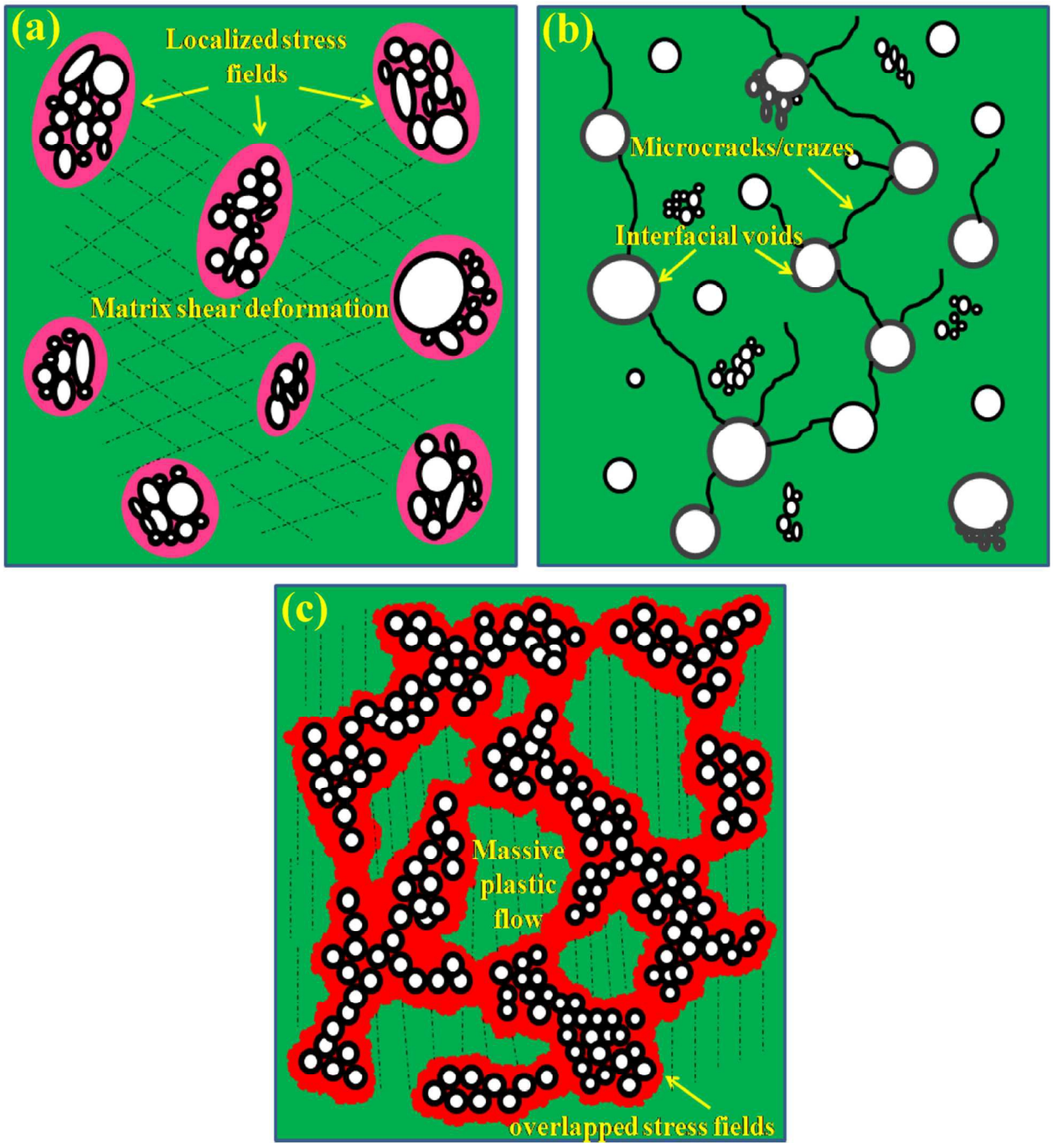

Fig. 14: Schematic representation of micromechanical deformations and toughening mechanisms in different ternary blends.(**a**) TR1 blend; (**b**) TR21 blend; (**c**) TR22 blend. The dispersed phases in different blends are exactly those denoted in Fig. 5.

4. Conclusions

Structure-property relationships were comprehensively studied for super-toughened PP-based reactive ternary blends, which were successfully prepared by melt blending of PP (70 wt%), EPDM-g-MA (15 wt%) and PA6 (15 wt%). Different phase morphologies were manipulated and their effects on the different properties of the resulting blends were thoroughly examined. TEM and SEM observations revealed core-shell phase morphology of PA6/EPDM-g-MA particles in reactive ternary blends but with quite different dispersion state of the complex structures in the PP matrix. A specific "percolated/interconnected" morphology of core-shell modifier particles was observed which showed significant enhancement in the impact toughness. This was attributed to a higher efficiency of the functionalized rubbery phase as both the interfacial modifier and toughening agent as compared to its effectiveness in other reactive blends. The phase structure, interfacial interactions, thermal properties and crystallinity of the blend systems were further investigated by DMA and DSC tests. These results mostly supported each other and in connection with other results showed that the phase morphology plays the key role in determining of different properties. The results of fractography study of the impact-fractured surfaces demonstrated the massive shear yielding and plastic deformation of matrix material as the main source of energy dissipation in toughened blends, which was triggered by more intense stress fields throughout the material followed by cavitation and plastic growth of micro-voids.

References

1. D. R. Paul, J. W. Barlow, H. Keskkula, in Encyclopedia of polymer science and engineering, H. F. Mark, N. M. Bikales, C. C. Overberger, G. Menges, Eds., 2nd ed.,Vol. 12. New York: Wiley-Interscience; 1988. p. 399.

2. Z. Li, P. A. Gonzalez Garza, E. Baer, C. J. Ellison, *Polymer,**2012,*** 53,3245-52.

3. L. L. Cui, C. Troeltzsch, P. J. Yoon, D. R. Paul, *Macromolecules,**2009,*** 42, 2599-2608.

4. T. D. Fornes, D. L. Hunter, D. R. Paul, *Macromolecules,**2004,*** 37, 1793-8.

5. M. H. Al-Saleh, U. Sundararaj,*Polymer,**2010,*** 51, 2740-7.

6. B. Yin, Y. Zhao, R. Z. Yu, H. N. An, M. B. Yang, *Polym. Eng. Sci.,**2007,*** 47, 14-25.

7. B. Yin, Y. Zhao, W. Yang, M. M. Pan, M. B. Yang, *Polymer,**2006,*** 47, 8237-40.

8. N. Virgilio, P. Desjardins, G. L'Esperance, B.D. Favis,*Macromolecules,**2009,*** 42, 7518-29.

9. Y. W. Mai, A. Dasari, Z. Z. Yu, *Macromolecules,**2007,*** 40, 123-30

10. A. R. Bhattacharyya, A. K. Ghosh, A. Misra, *Polymer,**2005,*** 46, 1661-74.

11.B. D. Favis, H. Liang, Y. S. Yu, A. Eisenberg, *Macromolecules,**1999,*** 32, 1637-42.

12. T. S. Valera, A. T. Morita, N. R. Demarquette, *Macromolecules,**2006,*** 39, 2663-75.

13. P. L. Corroller, B. D. Favis, *Polymer,**2011,*** 52, 3827-34

14. S. Ravati, B. D. Favis, *Polymer,**2010,*** 51, 4547-61

15. D. Wang, Y. Li, X. M. Xie, B. H. Guo, *Polymer,**2011,*** 52, 191-200.

16. S. Horiuchi, N. Matchariyakul, K. Yase, T. Kitano, *Macromolecules,**1997,*** 30, 3664-70

17. A. N. Wilkinson, L. Laugel, M. L. Clemens, V. M. Harding, M. Marin, *Polymer,**1999,*** 40, 971 –5

18. A. Wilkinson, M. L. Clemens, V. M. Harding, *Polymer,**2004,*** 45, 5239-49.

19. S. L. Bai, G. T. Wanga, J. M. Hiverb, C. G'Sell, *Polymer,**2004,*** 45, 3063-71

20. S. Y. Hobbs, M. E. Dekkers, V. H. Watkins, *Polymer,**1988,*** 29, 1598-602

21. H. F. Guo, S. Packirisamy, N. V. Gvozdic, D. J. Meier, *Polymer,**1997,*** 38, 785-94

22. M. M. Abolhasani, A. Arefazar, M. Mozdianfard*, J. Polym. Sci., Part B: Polym. Phys*., ***2010***, 48, 251-259.

23. L. P. Li, B. Yin, M. B. Yang, *Polym. Eng. Sci.,****2011,*** 51, 2425-33

24. L. P. Li, B. Yin, Y. Zhou, L. Gong, M. B. Yang, B. H. Xie, C. Chen, *Polymer, **2012,*** 53, 3043-51

25. B. Yin, L. P. Li, Y. Zhou, L. Gong, M. B. Yang, B. H. Xie, *Polymer, **2013,*** 54, 1938-47

26. R. Dou, W. Wang, Y. Zhou, L. P. Li, L. Gong, B. Yin, M. B. Yang, *J. Appl. Polym. Sci., **2013***, 129, 253-62.

27. R. Dou, W. Wang, Y. Zhou, L. Gong, B. Yin, M. B. Yang, *J. Appl. Polym. Sci., **2014**, 131,* 39937

28. R. Dou, Y. Zhou, C. Shen, L. Li, B. Yin, M. Yang, *Polym. Bull*.,***2015***, 72, 177-193.

29. Y. Zhou, W. Wang, R. Dou, L. P. Li, B. Yin, M. B. Yang, *Polym. Eng. Sci.,****2013,*** 53, 1845–55

30. Z. Zhang, X. Zhao, S. Wang, J. Zhang, W. Zhang, *RSC Adv.,****2014,*** *4,* 60617-25

31. C. Sanporean, Z. Vuluga, C. Radovici, D. M. Panaitescu, M. Lorga, J. Christiansen, A. Mosca, *RSC Adv.,****2014,*** *4,* 6573-79.

32. F. Chen, B. Qiu, B. Wang , Y. Shangguan, Q. Zheng, *RSC Adv.,****2015,*** *5, 20831*-37

33. R. Dou, C. Shen, B. Yin, M. Yang, B. Xie, *RSC Adv.,****2015,*** 5, 14592–14602.

34. C. Shen, Y. Zhou, R. Dou, W. Wang, B. Yin, M. Yang, *Polymer,****2015,*** 56, 395-405.

35. J. Rosch, R. Mulhaupt, *Makromol. Chem., Rapid Commun.,****1993***, 14, 503

36. J. Rosch, R. Mulhaupt, *Polym. Bull., **1994***, 32, 697-704

37. J. Rosch. R. Miilhaupt,*J. Appl. Polym. Sci.,****1995***, 56, 1599

38. J. Rosch, *Polym. Eng. Sci.,****1995***, 35(24), 1917

39. G. M. Kim, G. H. Michler, J. Rosch, R. Mulhaupt, *Acta Polymer, **1998***, 49, 88–95

40. G. M. Kim, G. H. Michler, M. Gahleitner, R. Mulhaupt, *Polym. Adv. Technol., **1998***, 9, 709-715

41. G. M. Kim, G. H. Michler, *Polymer,****1998,*** 39, 5699.

42. G. M. Kim, G.H. Michler, *Polymer,****1998,*** 39, 5689.

43. B. Ohlsson, H. Hassander, B. Tornell, *Polymer,**1998,*** 39 (26), 6705–6714

44. N. Zeng, S. L. Bai, C. G'Sell, J. M. Hiver, Y. W. Mai, *Polym. Int., **2002***, 51, 1439–1447

45. Y. Ou, Y. Lei, X. Fang, G. Yang, *J. Appl. Polym. Sci., **2004***, 91, 1806 –1815

46. H. Liu, T. Xie, Y.Ou, X. Fang, G. Yang, *Polym. J., **2004***, 36(9), 754-760

47. H. Liu, T. Xie, Y. Ou, X. Fang, G. Yang, *Polym. J., **2006***, 38(1), 21–30

48. H. Liu, T. Xie, Y. Zhang, Y.Ou, G. Yang, *J. Polym. Sci., Part B: Polym. Phys*.,***2006,*** 44, 1050–1061

49. M. M. Mazidi, M.K. Razavi Aghjeh, *RSC Adv., **2015***, 5, 47183.

50. S. Shokoohi, A. Arefazar, G. Naderi, *Mater.Des.,**2011,*** 32, 1697–1703

51. S. Shokoohi, A. Arefazar, G. Naderi, *Polym. Adv. Technol*.,***2012***, 23 418–424.

52. S. Wu, Polymer interface and adhesion. New York: Marcel Dekker; 1982.

53. I. Luzinov, C. Pagnoulle, K. Xi, G. Huynh-Ba, R. Jerome, *Polymer,**1999,*** 40, 2511.

54. C. A. Fleischer, A. R. Morales, J. T. Koberstein, *Macromolecules,**1994,*** 27, 379-385.

55. Y. S. Y. Fu, X. Q. Feng, B. Lauke, Y.W. Mai, *Compos. Part B-Eng.,**2008,*** 39(6), 933-61

56. L. Han, C. Han, L. Dong, *Polym. Compos.,**2013,*** 34, 122-130.

57. C. B. Bucknall, in *Toughened Plastics*; Applied Science Publishers: London, 1977.

58. A. J. Kinloch, R.J. Young, in *Fracture Behavior of Polymers*; Applied Science: London, 1983.

59. I. Walker, A. A. Collyer, in *Rubber Toughened Engineering Plastics*; Collyer, A. A., Ed.; Chapman & Hall: London, 1994; Chapter 2, p 29.

Structure-Property Relationships in Super-Toughened Polypropylene-Based Ternary Blends of Core-Shell Morphology

Majid Mehrabi Mazidi[1,2], Mir Karim Razavi Aghjeh[1,2]*, Hossein Ali Khonakdar[3], Uta Reuter[3]

Graphical Abstract: Super-toughened PP-based ternary blends were successfully prepared by reactive melt blending of PP/EPDM-g-MA/PA6 70/15/15. Different phase morphologies were manipulated and their effects on the properties of the resulting ternary blends were thoroughly examined. Core-shell phase morphology of PA6/EPDM-g-MA particles with quite different dispersion-states was observed in blends. A specific "percolated/interconnected" morphology of core-shell modifier particles resulted in tremendous enhancement in impact strength. Fracture behavior and toughening mechanisms were studied and proposed.

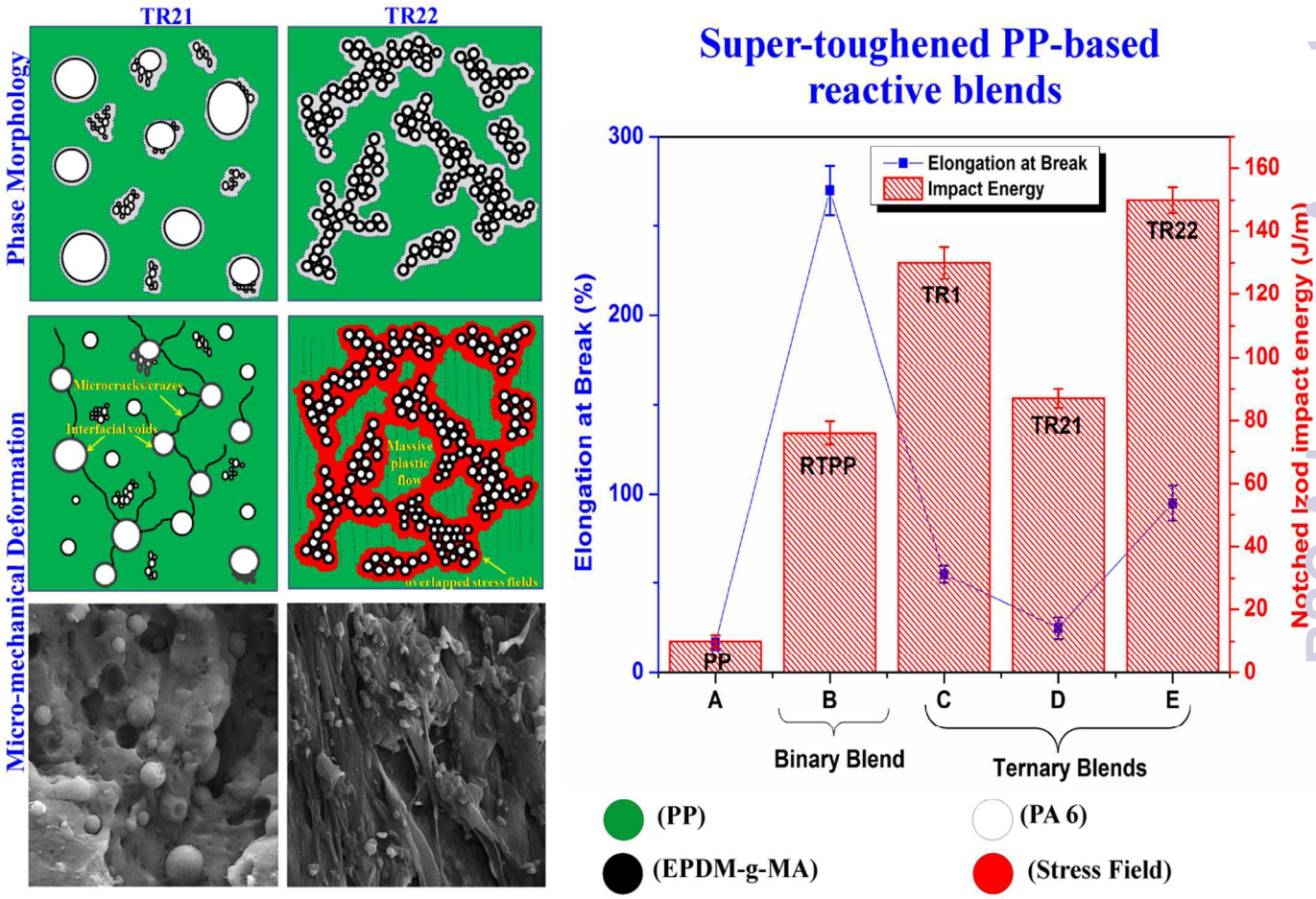

Graphical Abstract: Effect of Dispersion State of Core-Shell Particles in Super-Toughened PP-Based Ternary Blends